ornl

NUREG/CR-3888
ORNL/TM-9238

OAK RIDGE
NATIONAL
LABORATORY

MARTIN MARIETTA

Analysis of the Venus PWR Engineering Mockup Experiment - Phase I: Source Distribution

P. O. Morakinyo
M. L. Williams
F. B. K. Kam

Prepared for the
U.S. Nuclear Regulatory Commission
Office of Nuclear Regulatory Research
Under Interagency Agreement DOE 40-551-75 and 40-552-75

OPERATED BY
MARTIN MARIETTA ENERGY SYSTEMS, INC.
FOR THE UNITED STATES
DEPARTMENT OF ENERGY

Printed in the United States of America. Available from
National Technical Information Service
U.S. Department of Commerce
5285 Port Royal Road, Springfield, Virginia 22161

Available from

GPO Sales Program
Division of Technical Information and Document Control
U.S. Nuclear Regulatory Commission
Washington, D.C. 20555

NUREG/CR-3888
ORNL/TM-9238
Dist. Category R5

ANALYSIS OF THE VENUS PWR ENGINEERING MOCKUP EXPERIMENT - PHASE I: SOURCE DISTRIBUTION*

P. O. Morakinyo and M. L. Williams
Nuclear Science Center
Louisiana State University

F. B. K. Kam
Operations Division
Oak Ridge National Laboratory

Manuscript Completed - May 1984
Date Published - August 1984

*Prepared for the
U.S. Nuclear Regulatory Commission
Office of Nuclear Regulatory Research
Washington, D.C. 20555
under Interagency Agreements DOE 40-551-75 and 40-552-75

NRC FIN No. B0415

Prepared by the
Oak Ridge National Laboratory
Oak Ridge, Tennessee 37831
operated by
MARTIN MARIETTA ENERGY SYSTEMS, INC.
for the
U.S. DEPARTMENT OF ENERGY
under Contract No. DE-AC05-84OR21400

ACKNOWLEDGEMENT

The authors are grateful to the personnel of CEN/SCK in Mol, Belgium for providing the experimental measurements and other necessary data which enabled the goals of this study to be realized. The contributions of L. Leenders, G. Minsart, and A. Fabry were essential to the success of this study.

A major portion of this report describes work performed by the first author as partial fulfillment for a Master of Science degree at Louisiana State University (LSU). The support and aid of the LSU Nuclear Science Center is greatly appreciated.

This study was funded by the United States Nuclear Regulatory Commission (USNRC) and was supported by an Oak Ridge National Laboratory (ORNL) research subcontract with the LSU Nuclear Science Center.

TABLE OF CONTENTS

TABLE OF CONTENTS
(continued)

LIST OF TABLES

LIST OF TABLES
(continued)

LIST OF FIGURES

ABSTRACT

The neutron fission source distribution in the core of the VENUS PWR Mockup Experiment is computed and compared to experimental measurements. This experiment is an important component of the U.S. Nuclear Regulatory Commission's (USNRC's) program goal of benchmarking reactor pressure vessel (RPV) fluence calculations in order to determine the accuracy to which RPV damage can be computed. Of particular concern is the accuracy of the source calculation near the core-baffle interface, which is the important region for contributing to RPV fluence.

Calculations were performed with two-dimensional discrete ordinates transport theory, using cross sections based on ENDF/B-IV data. In addition to in-core fission rate calculations, several ex-core fission chamber responses were computed. The accuracy of the calculations were evaluated by comparison with the experimental measurements.

Results indicate that the calculated neutron source distribution within the VENUS core agrees with the experimentally measured values with an average error of less than 3%. At the important core-baffle interface, the agreement is within 3% error, except at the baffle corner, where the error is about 6%. The ex-core results are also in good agreement with measurements, except at the circular steel barrel, which was approximated into a rectangular geometry. It was discovered that a better accuracy in the calculations can be obtained by applying a detailed space dependent cross-section weighting procedure to the core-baffle interface region. Using this cross-section weighting in a two-dimensional transport theory calculation of a well-defined LWR core, the maximum error introduced into the predicted RPV fluence due to source errors should be on the order of 5%. However, in power reactor analysis, additional complexities (such as the time-dependent core composition and the use of few group diffusion theory) could affect this uncertainty value.

1. INTRODUCTION

The long-term potential for neutron embrittlement of reactor vessels has been a recognized concern of the nuclear industry for a number of years.[1] Recognition of pressurized water reactor (PWR) transients that could lead to severe thermal shock to the reactor pressure vessel (RPV), and the increasing awareness that some older plants are accumulating radiation damage at a faster rate than originally predicted have resulted in a re-evaluation of the RPV integrity during postulated overcooling accidents.[2]

There are indications that, under certain conditions, some postulated overcooling accidents could possibly result in pressure vessel failure, particularly if the transients occur late in the operating life of the vessel.[2] Of particular concern are several older reactors which contain large amounts of copper and nickel in the RPV welds. These reactor vessels are more susceptible to radiation embrittlement, whereby the ductile-to-brittle transition temperature of the vessel material is shifted to a higher temperature.[3] Injection of emergency core coolant in the core and other events that allow cool water to come in contact with the inner surface of the RPV could theoretically lower the RPV temperature below the nil ductility transition temperature. The rapid cooling of the inner surface, at a time when the primary system pressure is substantial, results in high RPV stresses, which, when coupled with reduction in the fracture toughness near the inner surface, introduces the possibility of propagation of pre-existent inner surface flaws. This possibility increases with reactor operating time due to the reduction in fracture toughness caused by neutron exposure.

In March 1982, the U.S. Nuclear Regulatory Commission (USNRC) officially declared the problem referred to as "pressurized thermal shock (PTS)" to be an unresolved safety issue.

To evaluate RPV integrity for both PTS and end-of-life (EOL) considerations, the need and importance of an accurate determination of the damage fluence accumulated by the RPV cannot be over-emphasized. Towards this end, the USNRC and the nuclear industry are currently conducting studies to determine the ability of PWR vessels to withstand severe thermal shocks without compromising their integrity. One of the major components of the USNRC research consists of benchmarking RPV fluence determination methods, since the RPV fluence is a main factor in the degree of radiation embrittlement.

An important part of the on-going RPV benchmark studies is called the "VENUS PWR Engineering Mockup Experiment." Calculations of this experiment were performed at the Louisiana State University (LSU) Nuclear Science Center under subcontract with the Oak Ridge National Laboratory (ORNL) and by CEN/SCK, Belgium. This experiment is one of a series of experiments which have been performed at various research reactors to validate particular aspects of RPV fluence calculations. A number of earlier experiments were performed at the Pool Critical Assembly (PCA,

the Oak Ridge Research Reactor Pool Side Facility (ORR-PSF), and the Bulk Shielding Reactor (BSR), all of which are located at ORNL. While these earlier experiments were useful in benchmarking the accuracy of ex-core transport calculations, they did not address the problem of validating the core fission source calculation, which drives the RPV fluence calculation. Of particular concern is the accuracy of the source distribution near the core-baffle interface, which is the important region for contributing to RPV fluence.

The PWR Engineering Mockup Experiment was designed primarily to address this problem. The experimental work is being performed by Centre d'Etude de l'Energie Nucleaire/Studie Centrum voor Kern Energie (CEN/SCK) at the VENUS Critical Facility in Mol, Belgium.

The objective of Phase I of this study is to accurately compute the VENUS core neutron source distribution, and to compare with measured values in order to contribute to USNRC's program goal of benchmarking RPV fluence calculations. The calculated fission source will be used in a later study as a fixed source for ex-core calculations, which will be performed in Phase II of the analysis. In addition to in-core measurements, U-235 and Np-237 fission chamber (dosimetry) measurements have been obtained, and some preliminary comparisons were made with ex-core calculations in the Phase I study.

The end results of this study contribute to the overall RPV embrittlement program by validating the accuracy of the neutron source calculation in PWR-like cores, which drives the determination of the RPV fluence. Uncertainties in the source distribution contribute to the uncertainty in the estimated vessel damage, which in turn results in an uncertainty in the ability of the RPV to withstand PTS transients. The specific tasks that were performed as part of the Phase I study are given by the following:

1. Generate few group cross sections that have been accurately weighted for the VENUS benchmark configuration. These cross sections will be available for future VENUS core calculations.
2. Perform discrete ordinates transport calculations to determine the neutron source for each pin in the VENUS core.
3. Examine the behavior of the thermal neutron flux near the core-baffle interface to determine the adequacy of a single thermal group.
4. Validate the accuracy of the calculational method by comparing the results with benchmark measurements.
5. Analyze the discrepancies associated with the results, and recommend procedures to improve the accuracy of the calculational methods for determining the core neutron source used in RPV fluence calculations.
6. Provide the neutron source results for subsequent use in calculating the transport of neutrons from the VENUS core to the barrel, neutron pad, and other ex-core positions.

2. EXPERIMENTAL CONFIGURATION

2.1 VENUS DESCRIPTION

The PWR benchmark configuration in the VENUS Critical Facility is shown in Fig. 1. The central portion of the geometry is water, surrounded by a 2.858-cm thick inner steel baffle. The inner core zone in the immediate vicinity of the inner baffle contains 752 zircaloy-clad, 3.3%-enriched fuel cells, with 48 pyrex rods interspersed among them. The outer core zone contains 1800 steel-clad, 4.0%-enriched fuel cells. The core itself is surrounded by a 2.858-cm thick outer steel baffle, a water reflector, a 4.972-cm thick steel core barrel, a water gap, a neutron pad, and the reactor pool.

The configuration shown in Fig. 1 was selected by Mol as the core loading best suited for the realization of the required measurements in the fuel zones, reflector, barrel, and up to the neutron pad. The distribution of pyrex rods in the inner zone of the core permits criticality without soluable boron in the water, and it shifts the power peak towards the core edges, thereby improving the core power distribution for the ex-core measurements. In addition, the use of water in the core center provides an interior zone of thermal neutrons for additional measurements, and it also shifts power towards the core edge. The 4.0% fuel pins (as opposed to the 3.3% fuel pins) were placed in the outer zone of the core to increase the fast flux levels in the pad, thus facilitating accurate measurements.[4]

2.2 VENUS SPECIFICATIONS

The characteristics of the fuel cells and the pyrex rods used in the VENUS benchmark configuration are specified in Tables 1 and 4, respectively. The chemical composition of the materials contained in the configuration are shown in Tables 2, 3, 5, 6, and 7. The material specifications are considered to be very accurate and were obtained by Mol using sophisticated and detailed methods.[5] Much effort has been devoted to insuring that this experiment is well characterized and of benchmark quality. It is possible that experimental results (e.g., the power distribution and criticality) for this exercise could be quite beneficial to other reactor physics benchmarking efforts (e.g., cross-section data testing) that are not directly related to the RPV embrittlement program.

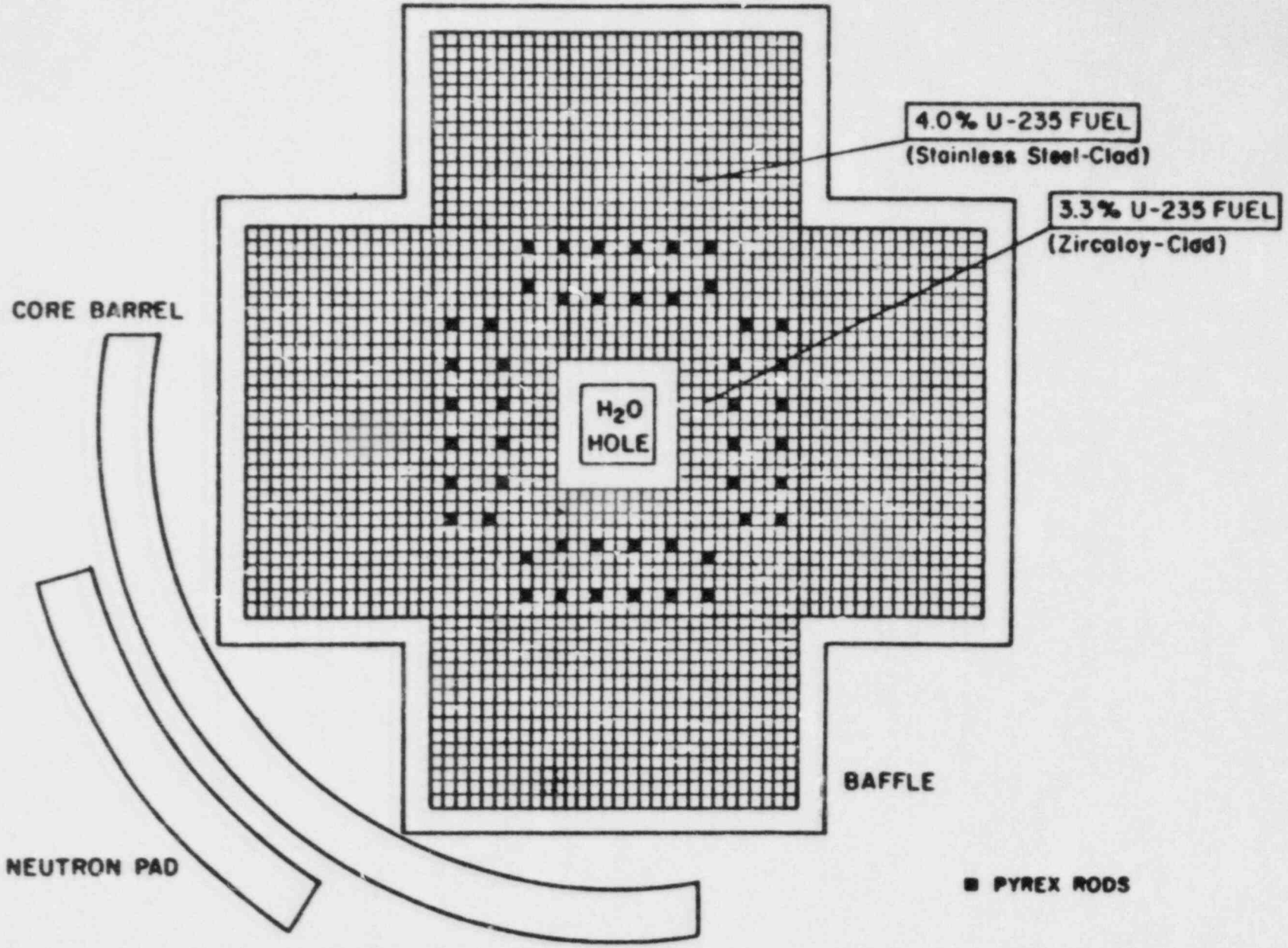

Fig. 1. VENUS benchmark configuration.

Table 1. Characteristics of the fuel cells used in the VENUS configuration

Characteristics		4.0%, U-235 enriched fuel	3.3%, U-235 enriched fuel
Stoichiometry:	(o/U+Pu)	2.000 ± 0.010	1.997 ± 0.005
Chemical composition of fuel (w/o)	UO_2	100.0	100.0
	PuO_2	0.0	0.0
Isotopic composition of uranium (w/o)	U-234	0.031 ± 0.009	0.029 ± 0.001
	U-235	4.022 ± 0.008	3.306 ± 0.010
	U-236	0.023 ± 0.006	0.016 ± 0.001
	U-238	95.924 ± 0.010	96.649 ± 0.012
Lattice pitch (cm):		1.260	1.260
Fuel diameter (cm):		0.8926 ± 0.0005	0.819 ± 0.002
Fuel length (cm):		50.0 ± 0.5	50.0 ± 0.1
Linear specific weight of fuel (gm/cm):		6.39 ± 0.07	5.40 ± 0.05
Cladding material:		SS-304	zircaloy-4
Cladding internal diameter (cm):		0.902 ± 0.004	0.836 ± 0.001
Cladding external diameter (cm):		0.978 ± 0.002	0.950 ± 0.001
Linear specific weight of cladding (gm/cm):		0.8855 ± 0.0007	1.0627 ± 0.0004
Number of available fuel cells:		1800	752

Table 2. Chemical composition of SS-304 cladding for the 4.0% fuel type

SS-304 elements	Chemical composition (w/o)	Atomic weight* (gm)
C	0.04 ± 0.04	--
Mn	1.29 ± 0.03	54.938
P	0.02 ± 0.02	--
S	0.015 ± 0.003	--
Si	0.135 ± 0.003	--
Cr	18.3 ± 0.4	51.996
Ni	10.03 ± 0.20	58.71
Mo	0.132 ± 0.003	--
Fe	70.038 ± 0.711	55.847

*Atomic weights are given for only the elements considered in the transport calculations.

Table 3. Chemical composition of zircaloy-4 cladding for the 3.3% fuel type

Zircaloy-4 elements	Chemical composition (w/o)	Atomic weight* (gm)
Fe	0.20 ± 0.01	--
Cr	0.10 ± 0.01	--
Sn	1.41 ± 0.06	118.69
O	0.12 ± 0.01	--
Zr	98.17 ± 0.06	91.22

*Atomic weights are given for only the elements considered in the transport calculations.

Table 4. Characteristics of the pyrex rods used in the VENUS configuration

Pyrex material:		Corning glass code 7740
Chemical composition (w/o):	SiO_2	78.53
	B_2O_3	14.65 ± 0.15
	Al_2O_3	2.21
	Fe_2O_3	0.05
	Na_2O_3	3.44
	K_2O_3	1.13
Isotopic composition of boron (at. %)	B-10	19.775 ± 0.005
	B-11	80.225 ± 0.005
Lattice pitch (cm):		1.260
Pyrex inner diameter (cm):		0.6058 ± 0.0031
Pyrex outer diameter (cm):		0.9048 ± 0.0045
Pyrex length (cm):		50.0 ± 0.1
Linear specific weight of pyrex (gm/cm):		0.7886 ± 0.0052
Cladding material:		SS-304
Cladding inner diameter (cm):		0.940 ± 0.003
Cladding outer diameter (cm):		0.978 ± 0.005
Specific weight of cladding (gm/cm^3):		7.9 ± 0.1
Number of available pyrex rods:		48

Table 5. Chemical composition of SS-304 cladding for the pyrex rod

SS-304 elements	Chemical composition (w/o)	Atomic weight* (gm)
C	0.03 ± 0.03	--
Mn	0.87 ± 0.42	54.938
Si	0.29 ± 0.16	--
Cr	18.4 ± 0.1	51.996
Ni	9.5 ± 0.5	58.71
Mo	0.07 ± 0.07	--
Fe	70.84 ± 1.28	55.847

*Atomic weights are given for only the elements considered in the transport calculations.

Table 6. Chemical composition of SS-304 baffle

SS-304 elements	Chemical composition (w/o)	Atomic weight* (gm)
C	0.04 ± 0.04	--
Mn	1.371 ± 0.441	54.938
P	0.022 ± 0.022	--
S	0.015 ± 0.015	--
Si	0.213 ± 0.040	--
Cr	16.37 ± 0.23	51.996
Ni	8.72 ± 0.15	58.71
Mo	0.457 ± 0.076	--
Fe	72.745 ± 0.343	55.847
Co	0.047 ± 0.070	--

*Atomic weights are given for only the elements considered in the transport calculations.

Table 7. Chemical composition of SS-304 barrel

SS-304 elements	Chemical composition (w/o)	Atomic weight* (gm)
C	0.015	--
Mn	1.303 ± 0.430	54.938
P	0.028	--
S	0.005	--
Si	0.513	--
Cr	18.464 ± 0.200	51.996
Ni	10.199 ± 0.380	58.71
Mo	0.474	--
Fe	68.819 ± 1.010	55.847
Co	0.097	--
N	0.080	--

*Atomic weights are given for only the elements considered in the transport calculations.

3. OVERVIEW OF CALCULATIONS

The procedural steps employed in calculating the space-dependent neutron source within the VENUS core are outlined below:

1. Determination of reactor parameters

   Using the given specifications, the atom densities of all important nuclides encountered in the core were calculated. Other reactor parameters such as dimensions, buckling, etc. were also determined, based on specifications provided by Mol. These values are given in Appendix A.

2. Fine-group, cross-section library

   A 218 neutron group, cross-section library[6] based on ENDF/B-IV nuclear data is used. The problem-independent, cross-section library contains a total of 65 different nuclides, which encompass all the necessary materials in the reactor.

3. Energy self-shielding calculation

   For each resonance nuclide encountered in the fuel region of the heterogeneous lattice unit cell, the flux in the absorber region is calculated with the Nordheim integral method. This weighting function is used to average the cross section of the resonance nuclide, in order to account for resonance shielding effects. This is discussed in Section 4.2.

4. Spatial self-shielding (or cell-averaging) calculation

   The disadvantage factor associated with the resonance shielded cross section in the fuel region is calculated and used to spatially average the group cross section over a unit cell. This is discussed in Section 4.2.

5. Collapse of fine-group cross sections

   The fine-group (218), cell-averaged cross sections are collapsed into a broad-group (10) structure, using a calculated, one-dimensional spectrum to flux weight the cross section. This is discussed in Section 4.3.

6. Eigenvalue calculation

   Using the broad-group cross sections, the total neutron source distribution is determined from a two-dimensional, k-eigenvalue calculation of the VENUS core, with the neutron flux normalized consistently with the experimental normalization. This is discussed in Section 5.

7. Fixed-source calculations

The neutron source distribution obtained from the eigenvalue calculation is used to perform a 56-group, fixed-source calculation. This is discussed in Section 5.

The overall calculations for the determination of the neutron source distribution in the VENUS configuration is summarized in the flow chart of Fig. 2.

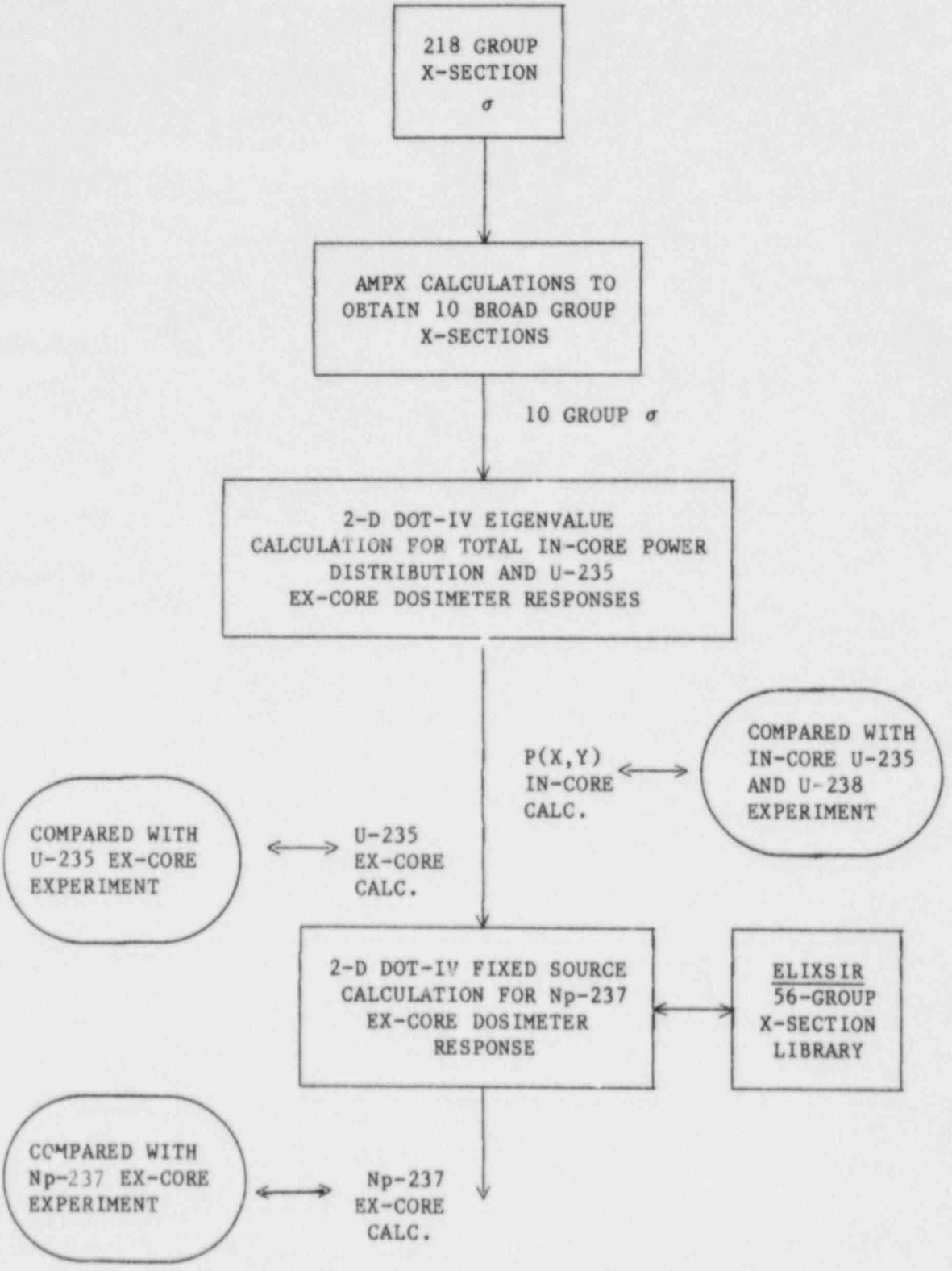

Fig. 2. Flow chart of the overall calculations.

4. METHODOLOGY FOR PROCESSING GROUP-DEPENDENT CROSS SECTIONS

4.1 DERIVATION OF CELL-AVERAGED MULTIGROUP CROSS-SECTION EQUATION

Cell theory

Consider a unit cell in the VENUS core lattice. Figure 3 shows a unit cell with a centrally located fuel pin surrounded by a moderator.

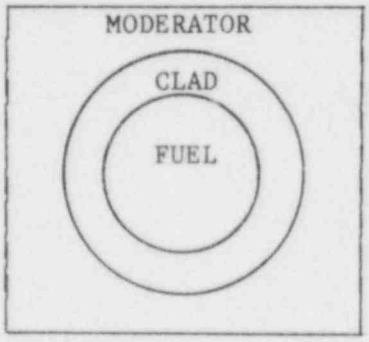

Fig. 3. A unit fuel cell.

The unit cell is heterogeneous; it has three homogeneous regions, namely the fuel, clad, and moderator. Consequently, we can determine the "equivalent homogenized" parameters spatially constant over the cell. These homogenized parameters will be equivalent in the sense that they will reproduce the average reaction rates throughout the cell. In essence, we are seeking "equivalent" group parameters that are constant over the volume occupied by any given cell making up the core and that, when used in an energy-dependent transport calculation for the whole core, will reproduce the same average reaction rates over a given cell in the reactor.

Cell-averaged equation

In order to account for localized pin heterogeneities, it is necessary that the core materials be cell-averaged. From cell theory*, the reaction rate in a cell is computed with cell-averaged cross sections defined to preserve the true reaction rate, i.e.,

$$\overline{\Sigma}^{i}_{c,g}\ \overline{\Phi}_{c,g}\ V_c = \int_{V_F}\int_{g} \Sigma^{i}_{F}(E)\Phi(r,E)dEdV + \int_{V_M}\int_{g} \Sigma^{i}_{M}(E)\Phi(r,E)dEdV \quad (1)$$

*For simplicity, the clad region is neglected in this discussion. The results can easily be generalized to three regions.

where $\bar{\Sigma}^i_{c,g}$ $\equiv$ cell-averaged macroscopic cross-section for group g of the i-th nuclide in the cell,

$\bar{\Phi}_{c,g}$ $\equiv$ cell-averaged flux for group g,

V_c $\equiv$ cell volume,

$\Sigma^i_F(E)$, $\Sigma^i_M(E)$ $\equiv$ energy-dependent macroscopic cross sections of the i-th nuclide in the fuel and moderator, respectively,

$\Phi(r,E)$ $\equiv$ space and energy-dependent flux.

Multiplying the first-term on the R.H.S. of Eq. (1) by $\frac{V_F}{V_F}$, and then by $\frac{\int_g \bar{\Phi}_F(E)dE}{\int_g \bar{\Phi}_F(E)dE}$, we have:

$$\int_{V_F} \int_g \Sigma^i_F(E)\Phi(r,E)dEdV = V_F \int_g \Sigma^i_F(E) \frac{\int_{V_F} \Phi(r,E)dV}{V_F} dE$$

$$= V_F \int_g \Sigma^i_F(E) \bar{\Phi}_F(E)dE$$

$$= V_F \frac{\int_g \Sigma^i_F(E) \bar{\Phi}_F(E)dE}{\int_g \bar{\Phi}_F(E)dE} \int_g \bar{\Phi}_F(E)dE$$

$$= V_F \bar{\Sigma}^i_{F,g} \bar{\Phi}_{F,g} \qquad (2)$$

where $\bar{\Sigma}^i_{F,g}$ $\equiv$ value of the cross section averaged over the fuel lump (and <u>not</u> over the entire unit cell) for group g,

$$\equiv \frac{\int_g \Sigma^i_F(E) \bar{\Phi}_F(E)dE}{\int_g \bar{\Phi}_F(E)dE} \quad , \text{ and}$$

$\bar{\Phi}_{F,g}$ $\equiv$ flux averaged over the fuel lump for group g.

In a similar manner, the second term on the R.H.S. of Eq. (1) can be expressed as:

$$\int_{V_M} \int_g \Sigma^i_M(E)\Phi(r,E)dEdV = V_M \bar{\Sigma}^i_{M,g} \bar{\Phi}_{M,g} \quad . \qquad (3)$$

Substituting Eqs. (2) and (3) into Eq. (1), we have:

$$\bar{\Sigma}^{i}_{c,g}\ \bar{\Phi}_{c,g}\ V_c = \bar{\Sigma}^{i}_{F,g}\ \bar{\Phi}_{F,g}\ V_F + \bar{\Sigma}^{i}_{M,g}\ \bar{\Phi}_{M,g}\ V_M \tag{4}$$

Notice that:

$$V_c = V_F + V_M \tag{5}$$

where V_F ≡ volume of the fuel region and

V_M ≡ volume of the moderator region.

The R.H.S. of Eq. (4) can be written in terms of microscopic cross sections as shown below:

$$\bar{\Sigma}^{i}_{c,g}\ \bar{\Phi}_{c,g}\ V_c = N^{i}_{F}\ \bar{\sigma}^{i}_{F,g}\ \bar{\Phi}_{F,g}\ V_F + N^{i}_{M}\ \bar{\sigma}^{i}_{M,g}\ \bar{\Phi}_{M,g}\ V_M \tag{6}$$

where N^{i}_{F}, N^{i}_{M} ≡ atom densities of the i-th nuclide in the fuel and moderator, respectively and

$\bar{\sigma}^{i}_{F,g}$, $\bar{\sigma}^{i}_{M,g}$ ≡ average microscopic cross sections of the i-th nuclide for group g in the fuel and moderator, respectively.

Rearranging Eq. (6) to solve for $\bar{\Sigma}^{i}_{c,g}$, we have:

$$\bar{\Sigma}^{i}_{c,g} = N^{i}_{F}\ \bar{\sigma}^{i}_{F,g}\ \frac{\bar{\Phi}_{F,g}}{\bar{\Phi}_{c,g}}\ \frac{V_F}{V_c} + N^{i}_{M}\ \bar{\sigma}^{i}_{M,g}\ \frac{\bar{\Phi}_{M,g}}{\bar{\Phi}_{c,g}}\ \frac{V_M}{V_c} \tag{7}$$

It can be seen from Eq. (7) that in order to obtain the cell-averaged cross section $\bar{\Sigma}^{i}_{c,g}$, it is necessary to know the zone-averaged cross sections $\bar{\sigma}^{i}_{F,g}$, $\bar{\sigma}^{i}_{M,g}$, and the flux ratios $\frac{\bar{\Phi}_{F,g}}{\bar{\Phi}_{c,g}}$, $\frac{\bar{\Phi}_{M,g}}{\bar{\Phi}_{c,g}}$

Each flux ratio is called an advantage or disadvantage factor, depending on whether it is greater or less than unity, respectively.

4.2 ENERGY AND SPATIAL SELF SHIELDING

Nuclides with resonance effects are usually associated with materials in the fuel region. The complexity of the heterogeneous lattice treatment stems from the fact that the flux in the resonance region is a function of both energy and space. To account for localized pin heterogeneities, it becomes necessary that the core materials be resonance shielded and cell averaged.

Energy self shielding - NITAWL

The fuel group cross sections ($\sigma^{i}_{F,g}$) associated with the first term on the R.H.S. of Eq. (7) must be resonance shielded, as implied by Eq. (2).

By averaging the actual cross-section data over the various energy groups, with the scalar flux as a weighting function, we can compute the shielded, problem-dependent cross sections, i.e.,

$$\bar{\sigma}^{i}_{F,g} = \frac{\int_{g}^{g-1} \bar{\Phi}_F(E)\sigma^{i}(E)dE}{\int_{g}^{g-1} \bar{\Phi}_F(E)dE} \tag{8}$$

where $(g, g-1)$ Ξ energy interval of the g-th energy group,
$\sigma^{i}(E)$ Ξ actual cross section data for nuclide i, and
$\bar{\Phi}_F(E)$ Ξ energy-dependent flux for weighting (to be computed).

In the resonance energy range, $\bar{\Phi}_F(E)$ and $\sigma^{i}(E)$ may both vary drastically, and the flux weighting, referred to as "energy self shielding (or resonance shielding)" is most important.

The scalar flux of Eq. (8) was determined for each fuel type by using the Nordheim[7] integral method, which basically solves an expression for the collision density in the fuel lump. The Nordheim integral treatment solves the integral slowing down equation for the energy dependent flux in a material region that contains a resonance absorber (i.e., fuel lump) and a maximum of two admixed moderators. The presence of more than one absorber in the moderating region (i.e., a fuel pin lattice) is accounted for through the use of a Dancoff-Ginsberg correction factor. The collision density equation solved by the Nordheim method can be written as:

$$\bar{\Sigma}_{tF}(E)\,\bar{\Phi}_F(E) = \sum_{i=1}^{3}\left[\frac{1-P^{*}_{FO}(E)}{1-\alpha^{i}_{F}}\int_{E}^{E/\alpha^{i}_{F}} \Sigma^{i}_{SF}(E')\,\bar{\Phi}_F(E')\,\frac{dE'}{E'} + \frac{P^{*}_{FO}(E)\,\Sigma_{tF}(E)}{\bar{\xi}\bar{\Sigma}_{s}}\right] \tag{9}$$

where $\Sigma_{tF}(E)$ Ξ total macroscopic cross section of the fuel at energy E,
$\bar{\Phi}^{i}_{F}(E)$ Ξ average flux in the fuel at energy E,
i Ξ nuclide index:
i = 1 for the absorber
i = 2 for the first admixed moderator in the fuel
i = 3 for the second admixed moderator in the fuel

$\alpha_F^i \left(\frac{A_F^i - 1}{A_F + 1} \right)^2$, A_F^i $\equiv$ mass of the i-th nuclide contained in the fuel region

$P_{FO}^*(E)$ $\equiv$ Dancoff-Ginsberg corrected first-flight escape probability for the absorber region

$\sum_{sF}^i(E')$ $\equiv$ macroscopic scattering cross section of the i-th nuclide colliding in the fuel region at energy E',

$\bar{\Phi}_F(E')$ $\equiv$ average flux in the fuel at energy E',

$\sum_{tF}^i(E)$ $\equiv$ total macroscopic cross section of the i-th nuclide in the fuel region at energy E

$\bar{\xi}$ $\equiv$ average logarithmic energy decrement

$\bar{\sum}_s$ $\equiv$ average macroscopic moderator scattering cross section

The Nordheim's method is implemented in the NITAWL[8,9] code, where each resonance is treated independently. For each resonance, the flux in the absorber region is obtained by numerical integration over a fine energy mesh (of lethargy intervals), with slowing down sources due to the absorber and the two admixed moderators explicitly calculated as in Eq. (9). Having determined the scalar flux for each fuel type, the shielded (resolved) cross sections represented by Eq. (8) are subsequently calculated. Details of the Nordheim integral treatment can be found in Ref. 7.

Spatial self-shielding (cell-averaging) - XSDRNPM

The energy shielded cross section can be used to homogenize the unit cell by multiplying by the associated flux ratios $\frac{\Phi_{F,g}}{\Phi_{c,g}}$ and $\frac{\Phi_{M,g}}{\Phi_{c,g}}$ of Eg. (7). A multiplication of the energy shielded cross section by the flux ratio constitute spatial self shielding of the cross section (or spatial cross-section weighting).

The flux ratios were calculated with a one-dimensional discrete ordinates code called XSDRNPM.[10] This code numerically solves the time-independent Boltzmann equation in one-dimension with the coordinate system of interest.

The square unit cell was modeled into a cylindrical Wigner-Seitz unit cell of mixtures and zones with appropriate spatial intervals. The cylindrical geometries for the 3.3 and 4.0% fuel types and for the pyrex rod are shown in Figs. 4, 5, and 6, respectively. In the XSDRNPM weighting calculation, the "cell weighting" option was used for the fuel cells, while the "inner cell weighting" option was used for the pyrex rod. The XSDRNPM calculations were based on S8-P3 transport approximation.

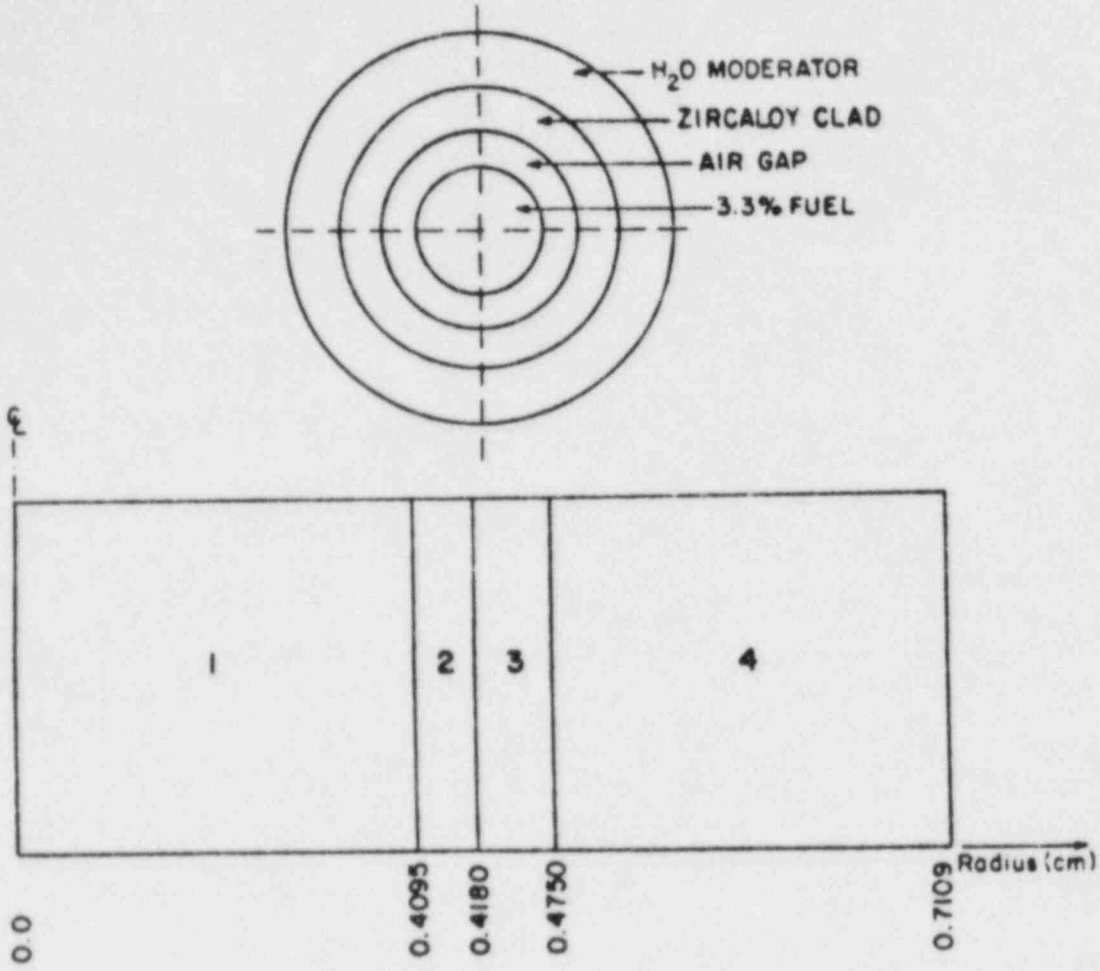

Definition:

Zone	Composition	No. of spatial intervals
1	3.3% fuel pellet	10
2	Air gap	1
3	Zircaloy clad	1
4	H_2O moderator	10

Fig. 4. 3.3% fuel cell geometry for cross-section averaging.

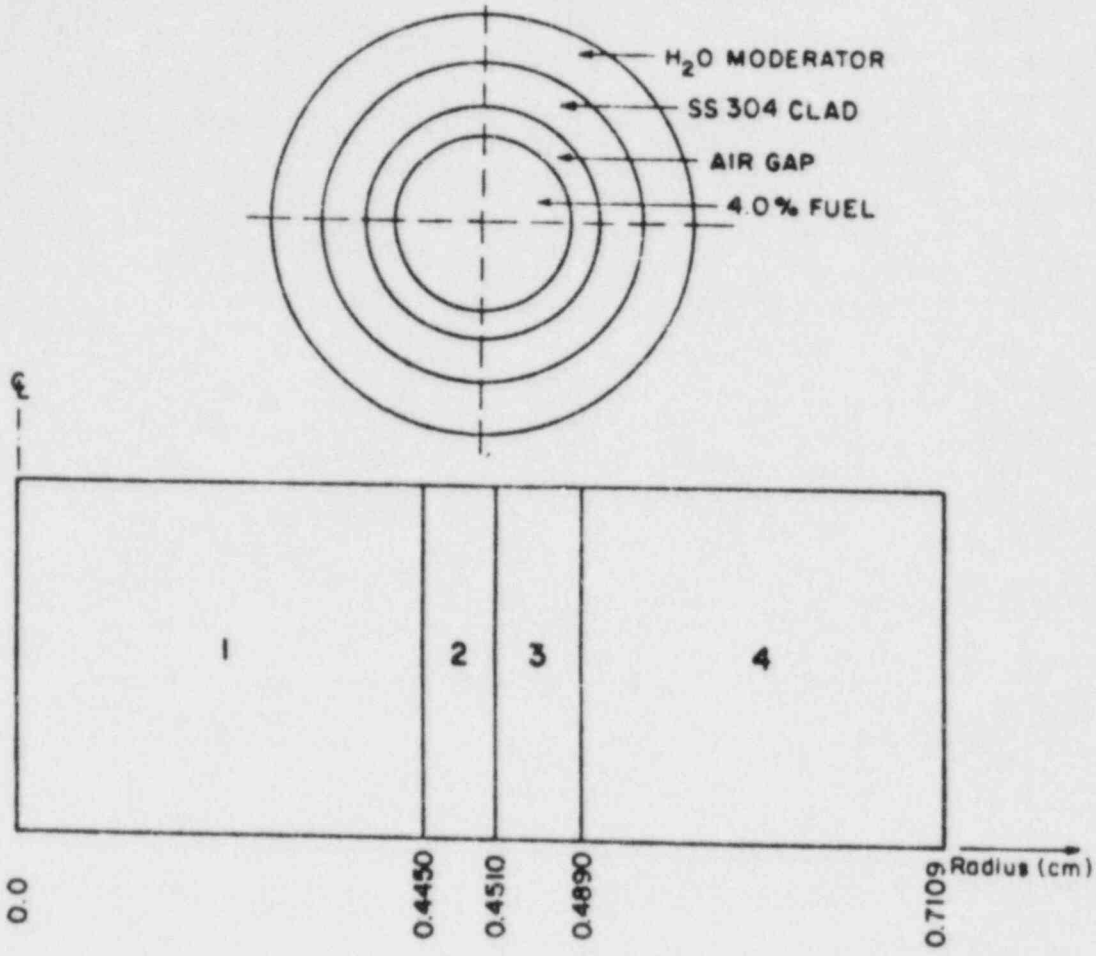

Definition:

Zone	Composition	No. of spatial intervals
1	4.0% fuel pellet	10
2	Air gap	1
3	SS-304 clad	1
4	H_2O moderator	10

Fig. 5. 4.0% fuel cell geometry for cross-section averaging.

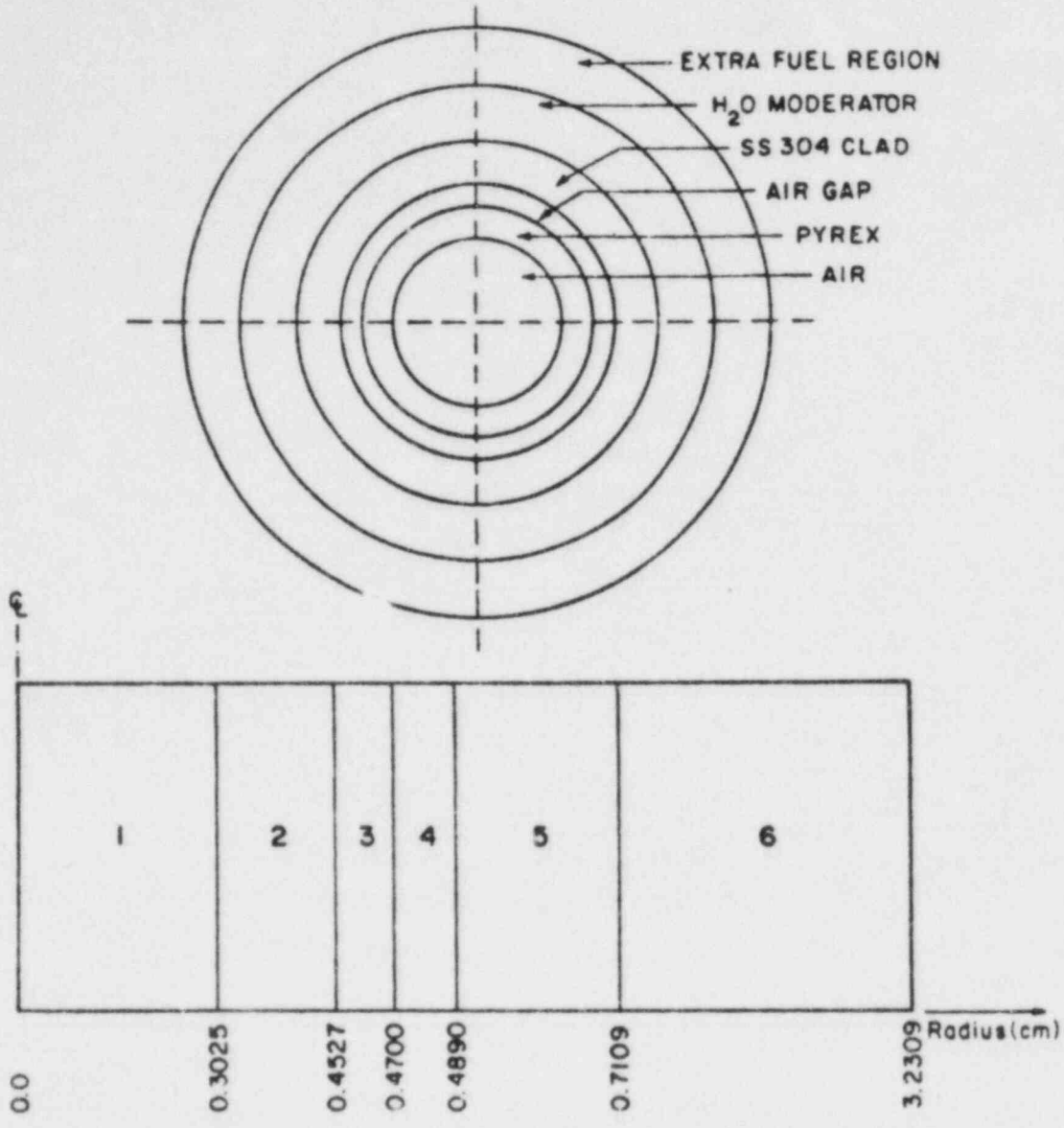

Definition:

Zone	Composition	No. of spatial intervals
1	Air	10
2	Pyrex	5
3	Air gap	1
4	SS-304 clad	1
5	H_2O moderator	10
6	Extra fuel region	30

Fig. 6. Pyrex cell with extra fuel cell geometry or cell calculation.

4.3 CROSS-SECTION COLLAPSING

After cell homogenization, the XSDRNPM code was again used to perform a one-dimensional, 218-group transport theory calculation in order to obtain zone weighting spectra. Fig. 7 corresponds to the one-dimensional cylindrical model of the VENUS configuration used in the calculation. The weighting spectra were then used to zone-wise collapse the 218 fine-group cross section into 10 broad groups, with the energy boundaries of Table 8. The 218-group cross sections contain 78 thermal groups, which permit an accurate calculation of the thermal spectrum used in averaging the single thermal group of the 10-group structure. It should be noted that the single inner 3.3% and the seven outer 4.0% zones of Fig. 7 are boundary zones, which have been used to account for the change in the thermal spectrum near the core-baffle interfaces.

The expression for the collapsed zone dependent, broad-group cross section can be written as:

$$\bar{\Sigma}_{cG}(Z) = \frac{\sum_{g \epsilon G} \bar{\Sigma}_{c,g} \bar{\Phi}_g(Z)}{\sum_{g \epsilon G} \bar{\Phi}_g(Z)} \qquad (10)$$

where $\bar{\Phi}_g(Z)$ is the zone-averaged flux spectrum calculated from the one-dimensional model of the VENUS configuration, g is the fine-group index, and G is the broad-group index.

4.4 FLOW CHART OF CALCULATIONS

The AMPX[11] modular system was used for all the cross-section processing calculations. The AMPX system is a collection of computer programs in a modular arrangement for processing cross-section data. The modularity is particularly attractive, since it allows the user to choose an arbitrary execution sequence from the modules available in the system. Details of the AMPX system can be found in Ref. 11.

A flow chart of the various AMPX modules used in the cross-section processing calculations is shown in Fig. 8.

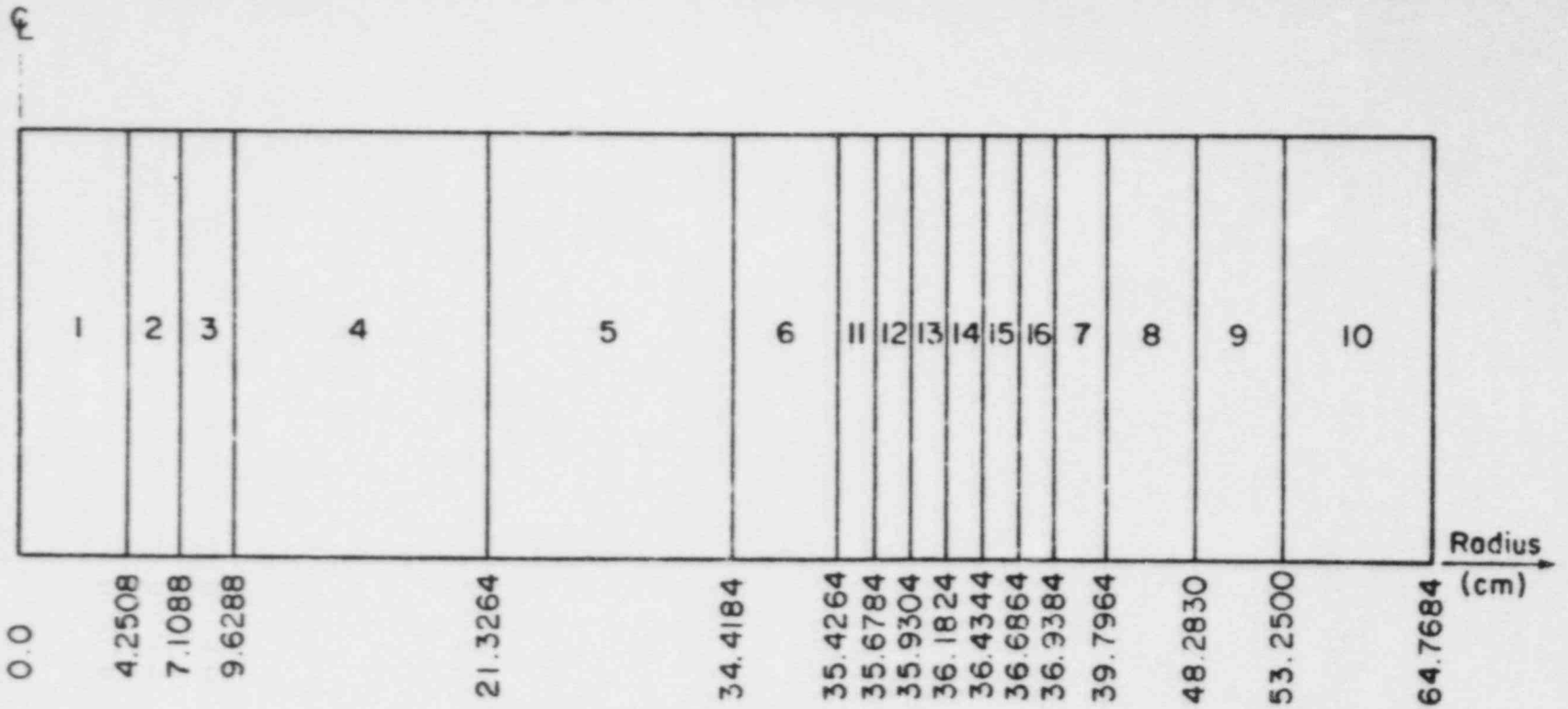

Definition:

Zone	Description	Composition	No. of Spatial intervals
1	Water hole	Water	15
2	Inner baffle	SS-304	10
3	Inner 3.3% fuel	3.3% fuel + pyrex	10
4	Outer 3.3% fuel	3.3% fuel + pyrex	22
5	Inner 4.0% fuel	4.0% fuel	25
6	Outer 4.0% fuel	4.0% fuel	4
7	Outer baffle	SS-304	10
8	Reflector	Water	22
9	Simulated barrel	SS-304	10
10	Water pool	Water	12
11-16	Outer 4.0% fuel	4.0% water	6

Fig. 7. 1-D cylindrical model of the VENUS configuration.

Table 8. 10-group energy structure used in the 2-D eigenvalue calculation

Broad group	Fine groups	Upper energy (eV)	Lower lethargy	Fission spectrum*
1	1-7	2.00E+07	-0.6931	4.250E-01
2	8-33	1.85E+06	1.6870	5.137E-01
3	34-46	2.70E+05	3.6120	5.876E-02
4	47-53	3.00E+04	5.8090	2.407E-03
5	54-66	3.90E+03	7.8490	1.135E-04
6	67-83	5.50E+02	9.8080	6.055E-06
7	84-124	7.20E+01	11.8400	2.856E-07
8	125-154	1.00E+01	13.8200	1.434E-08
9	155-191	1.86E+00	15.5000	9.921E-10
10**,†	192-218	6.50E-01	16.5500	2.583E-10

*This is an ENDF/B-IV fission spectrum resulting from the ENDF/B-IV cross-section data. An ENDF/B-V based fission spectrum was used in the 2-D calculation, for better accuracy.

**Lower energy of group 10 = 1.00E-05 eV.

†Upper lethargy of group 10 = 27.63.

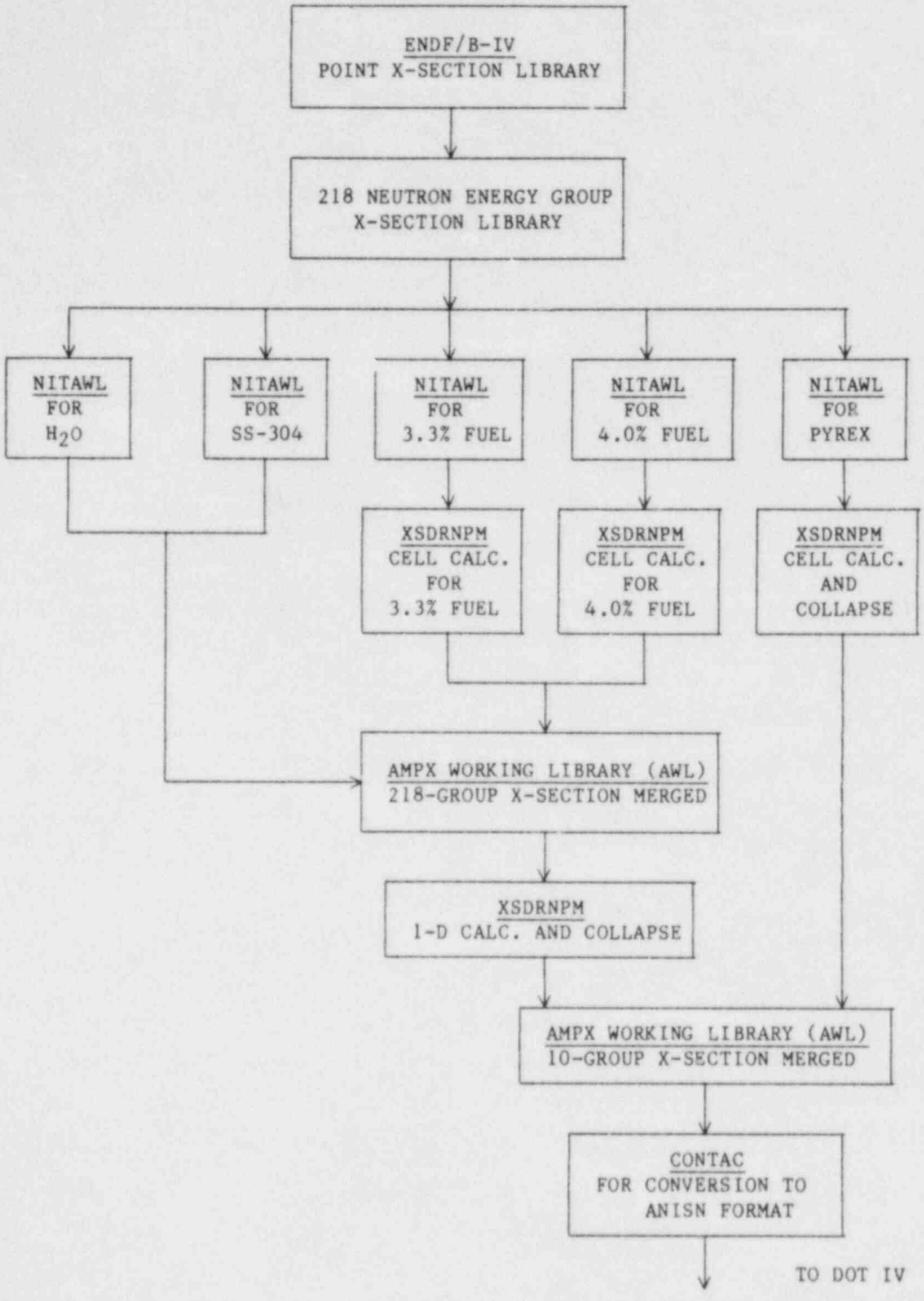

Fig. 8. Flow chart of AMPX modules for cross-section processing.

5. METHODOLOGY FOR FISSION RATE CALCULATION

5.1 EIGENVALUE CALCULATION

The total fission source distribution in the VENUS core was determined from a k-eigenvalue calculation of the reactor core. The DOT IV[12] code was used to perform a two-dimensional X-Y calculation of the critical eigenvalue. DOT IV is a two-dimensional discrete ordinates code which numerically solves the Boltzmann transport equation. The Boltzmann equation, which is a mathematical expression of the neutron-balance condition, is solved for the flow of neutrons moving in a set of discrete directions in each interval of a space mesh, and in each group of multigroup energy structure. Since the neutron balance condition must be maintained over an arbitrary spatial region, energy interval, and discrete direction, DOT IV produces an accounting of the various production and loss mechanism within a specified zone or region.

A two-dimensional form of the Boltzmann transport equation solved by DOT IV in rectangular coordinates can be expressed as:

$$\Omega_x \frac{\partial}{\partial_x}[\Psi(s,y,E,\Omega)] + \Omega_y \frac{\partial}{\partial_y}[\Psi(x,y,E,\Omega)] + \Sigma_t(x,y,E)\Psi(x,y,E,\Omega)$$

$$= \int_{E'} \int_{\Omega'} \Sigma_s(x,y,E' \to E, \Omega' \to \Omega)\, \Psi(x,y,E',\Omega')d\Omega' dE' + S(x,y,E,\Omega) + Q(x,y,E,\Omega)$$

where: Ω_x, Ω_y $\equiv$ direction cosines of the unit direction vector Ω, $= \vec{i}.\Omega$ and $\vec{j}.\Omega$, respectively

$\Psi(x,y,E,\Omega)$, $\Psi(x,y,E',\Omega')$ $\equiv$ angular fluxes

$\Sigma_t(s,y,E)$ $\equiv$ total macroscopic cross section

$\Sigma_s(x,y,E' \to E, \Omega' \to \Omega)$ $\equiv$ angular dependent scatter cross section for a neutron of energy E' in direction Ω' scattering into energy E in direction

$$S(x,y,E,\Omega) = X(E) \int_{E'} \int_{\Omega'} \nu \Sigma_f(x,y,E')\Psi(x,y,E',\Omega')d\Omega' dE'$$

$\equiv$ fission source

$Q(x,y,E,\Omega)$ $\equiv$ fixed (or external) source

$X(E)$ $\equiv$ fission spectrum

$\nu(E')$ $\equiv$ average number of neutrons per fission

$\Sigma_f(x,y,E')$ $\equiv$ macroscopic fission cross section

For the two-dimensional calculation, the VENUS benchmark configuration was modeled in X-Y rectangular coordinates since the fuel cells are loaded in a rectangular pitch. Due to the fact that this is a core calculation, the model was terminated at the core barrel. The fact, that rectangular coordinates were used, required that the circular steel barrel be approximated as a "stair-step." The model used in the two-dimensional calculations is shown in Fig. 9. The model was divided into zones as shown in Fig. 10, and the corresponding descriptions are given in Table 9. Notice that as in the one-dimensional model, boundary zones have been included at the inner and outer core boundaries in order to use the appropriately weighted cross sections.

Before the DOT IV calculation was performed, the 10-group macroscopic cross sections obtained earlier were combined into the appropriate macroscopic mixture cross sections, using the cell homogenized atom density values of Table 10.

The DOT IV eigenvalue calculation was performed with a P_3 Legendre expansion of the cross sections and an S_8 quadrature set. The weighted flux differencing scheme was used and the calculation was accelerated with the diffusion acceleration option. The VENUS model, as shown in Figs. 9 and 10, contains 103 mesh intervals in both the X and Y directions. The internal boundaries are as depicted in Table 11. Leakage in the axial direction was treated with a buckling approximation (DB^2 losses), using a buckling value of $B^2 = 24 \times 10^{-4}$ cm^{-2}.

Using the appropriate diffusion coefficient values, the DB^2 values were determined and tabulated in Table 12. See Appendix A for the method used to compute the diffusion coefficients. An ENDF/B-V[13] (as opposed to the ENDF/B-IV) based fission spectrum of Table 13 was used in the 2-D calculation for better accuracy. Other necessary input arrays were determined, and entered into DOT IV. A flow chart of the DOT IV input and output scheme is shown in Fig. 11.

The eigenvalue was calculated to be $k_{eff} = 0.996$, which is quite reasonable. On the basis of the 10-group fluxes obtained from the eigenvalue calculation, the space-dependent, total fission rate (for both U-235 and U-238) at each point within the core of the VENUS model was computed. In addition, activities for the U-235 fission rate in steel were calculated. Fission chamber activities for specified detector locations were computed, using the interpolation method of Taylor polynominal.

In order to compare the calculated fission rate values with the experimental measurements from Mol, it became necessary that the results be normalized consistently. The normalization process was effected by first calculating the total fission rate (for both U-235 and U-238), integrated over the entire reactor core. This value was then divided by the total number of cells in the core to determine the average fission rate per cell. Finally, the calculated space-dependent fission rate at each point in the reactor core was divided by the average fission rate per cell to obtain the relative power distribution. The normalization of the calculated and measured fission chamber results was different than that for the core power distribution. In this case, the results were both normalized to 1.0 at a specified position in the inner baffle. The absolute fission rate in the VENUS core was not known at the time this study was performed.

ORNL DWG 83-16515

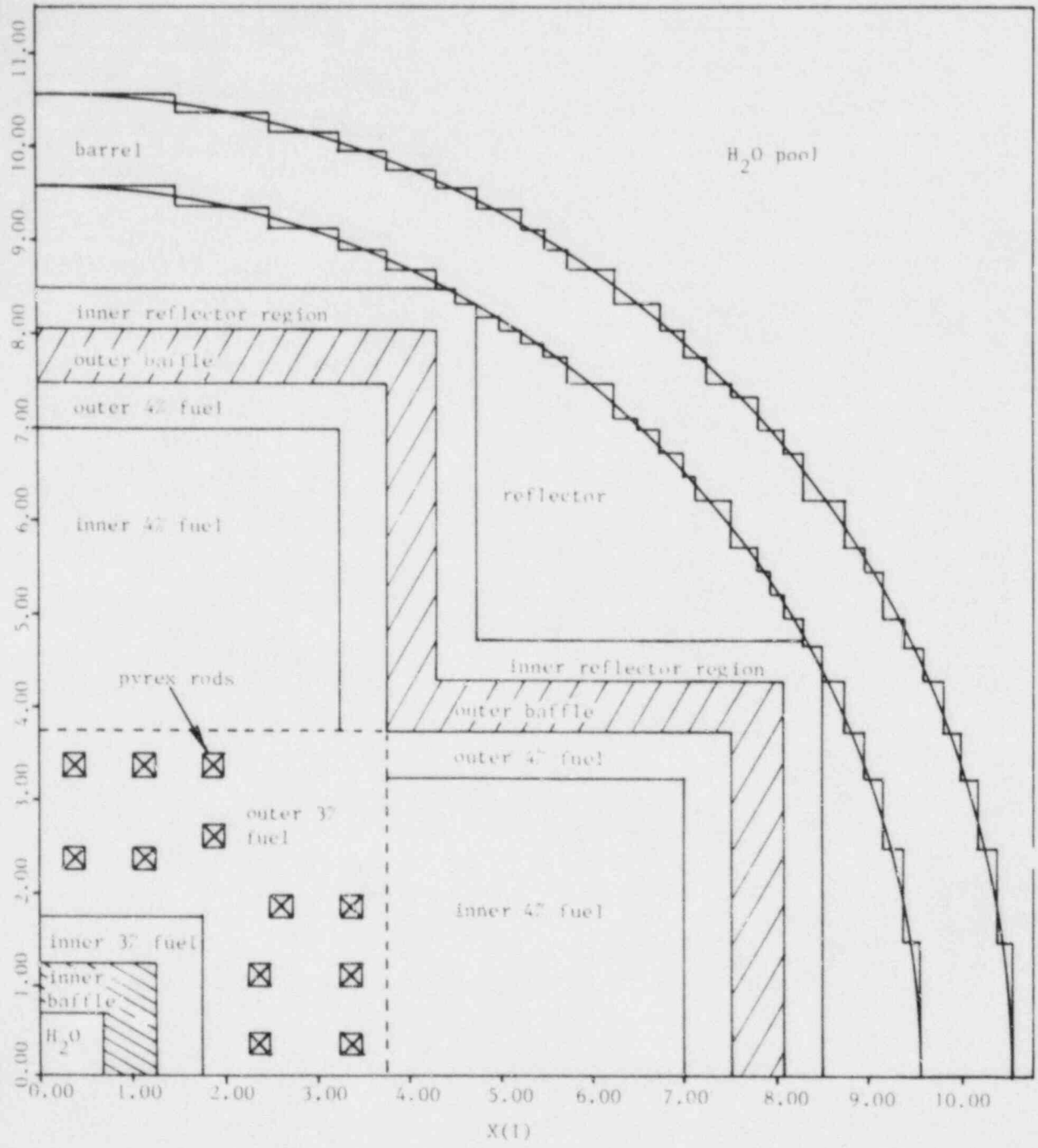

Fig. 9. 1/4 core of the VENUS 2-D rectangular model (Scale: 1 unit = 4 pin pitches = 5.04 cm).

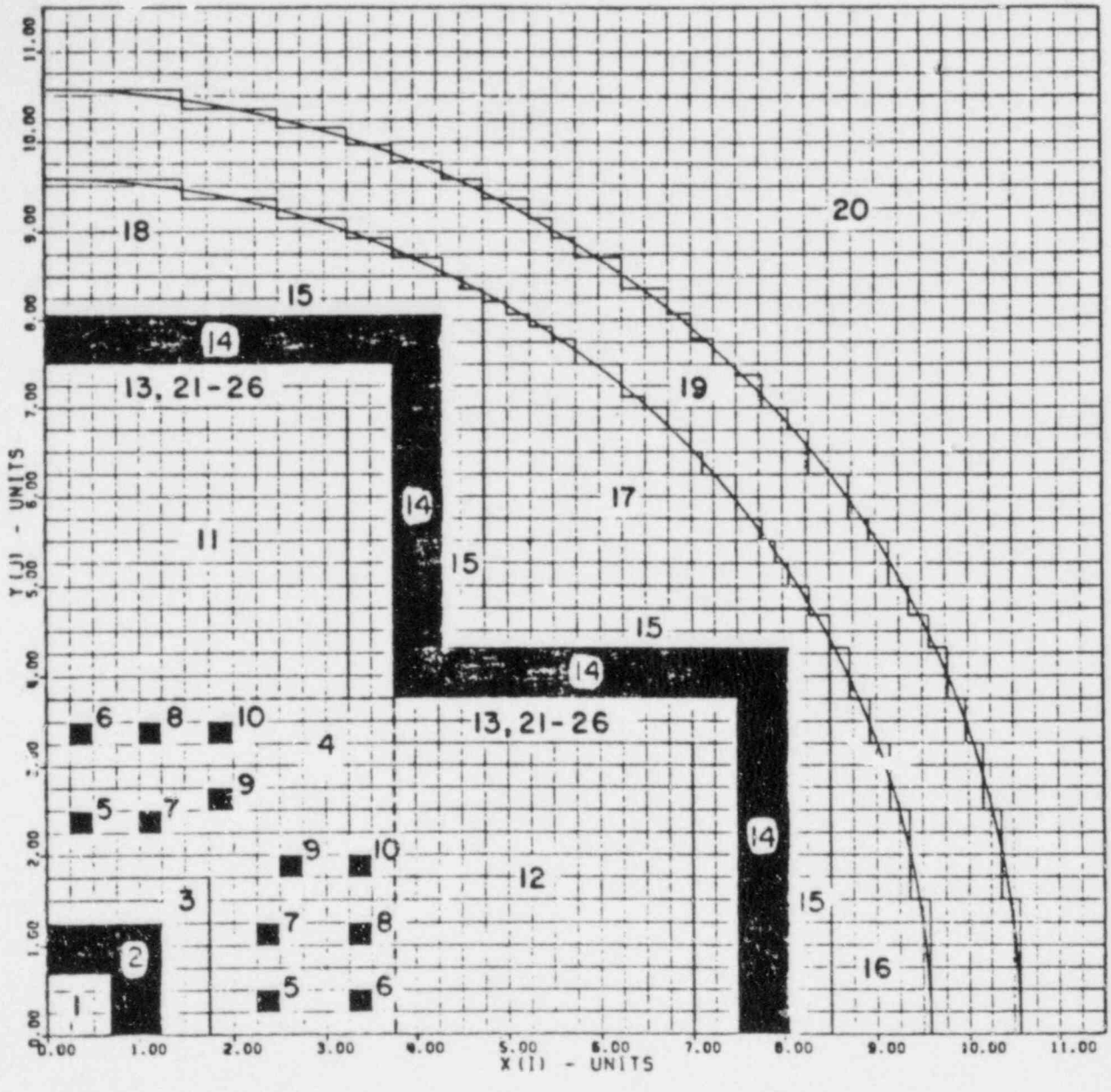

Fig. 10. Zones used in the VENUS 2-D eigenvalue calculation (Scale: 1 unit = 4 pin pitches = 5.04 cm).

Table 9. Definition of the zones used in the VENUS 2-D eigenvalue calculation

Zone	Description	Composition
1	Water hole	H_2O
2	Inner baffle	SS-304
3	Inner 3.3% fuel	3.3% fuel
4	Outer 3.3% fuel	3.3% fuel + pyrex
5-10	Pyrex	Pyrex
11-12	Inner 4.0% fuel	4.0% fuel
13	Outer 4.0% fuel	4.0% fuel
21-26	Outer 4.0% fuel	4.0% fuel
14	Outer baffle	SS-304
15	Inner reflector	H_2O
16-18	Outer reflector	H_2O
19	Barrel	SS-304
20	Water pool	H_2O

Table 10. Atom densities of the mixtures used in the VENUS 2-D calculations

Mixture	Nuclide	N ($\frac{\text{atoms}}{\text{barn-cm}}$)
H_2O	H	6.68652E-02
	O	3.34326E-02
SS-304 baffle	Mn	1.18770E-03
	Cr	1.49840E-02
	Ni	7.06890E-03
	Fe	6.19945E-02
3.3% fuel + Zircaloy cladding + H_2O	U-234	2.22330E-06
	U-235	2.54050E-04
	U-236	1.22780E-06
	U-238	7.33343E-03
	Sn	4.78945E-05
	Zr	4.33881E-03
	H	3.70110E-02
	O	3.36790E-02
4.0% fuel + SS-304 cladding + H_2O	U-234	2.83120E-06
	U-235	3.65740E-04
	U-236	2.08270E-06
	U-238	8.61280E-03
	Mn	7.88830E-05
	Cr	1.18235E-03
	Ni	5.73925E-04
	Fe	4.21310E-03
	H	3.52260E-02
	O	3.55680E-02
Pyrex + SS-304 cladding + H_2O	Si	3.91030E-03
	B-10	2.48980E-04
	B-11	1.01010E-03
	Al	1.29690E-04
	Na	3.32105E-04
	K	7.17700E-05
	Mn	2.71684E-05
	Cr	6.07112E-04
	Ni	2.77610E-04
	Fe	2.17809E-03
	H	3.52260E-02
	O	2.77215E-02

Table 11. Mesh intervals used in the 2-D eigenvalue calculation

Interval boundary No.	Distance (cm)	Internal midpoint (cm)	Internal width (cm)
1	0.0	3.15000E-01	6.30000E-01
2	6.30000E-01	9.44999E-01	6.30000E-01
3	1.26000E+01	1.41750E+00	3.15000E-01
4	1.57500E+00	1.73250E+00	3.15000E-01
5	1.89000E+00	2.04750E+00	3.15000E-01
6	2.20500E+00	2.36250E+00	3.15001E-01
7	2.52000E+00	2.75050E+00	4.61000E-01
8	2.98100E+00	3.21150E+00	4.61000E-01
9	3.44200E+00	3.64175E+00	3.99499E-01
10	3.84150E+00	4.04125E+00	3.99500E-01
11	4.24100E+00	4.44075E+00	3.99500E-01
12	4.64050E+00	4.84025E+00	3.99500E-01
13	6.50000E+00	5.19750E+00	3.15000E-01
14	5.35500E+00	5.51250E+00	3.15000E-01
15	5.67000E+00	5.82750E+00	3.15000E-01
16	6.98500E+00	6.14250E+00	3.15001E-01
17	6.30000E+00	6.61500E+00	6.30000E-01
18	6.93000E+00	7.24500E+00	6.30000E-01
19	7.56000E+00	7.87500E+00	6.30000E-01
20	8.19000E+00	8.50500E+00	6.30000E-01
21	8.82000E+00	8.97750E+00	3.15000E-01
22	9.13500E+00	9.29250E+00	3.15000E-01
23	9.45000E+00	9.60750E+00	3.15000E-01
24	9.76500E+00	9.92250E+00	3.15001E-01
25	1.00800E+01	1.07100E+01	1.26000E+00
26	1.13400E+01	1.14975E+01	3.15000E-01
27	1.16550E+01	1.81250E+01	3.15000E-01
28	1.19700E+01	1.21275E+01	3.15000E-01
29	1.22850E+01	1.24425E+01	3.15001E+00
30	1.26000E+01	1.27575E+01	3.15000E-01
31	1.29150E+01	1.30725E+01	3.15001E-01
32	1.32300E+01	1.33875E+01	3.15000E-01
33	1.35450E+01	1.37025E+01	3.15001E-01
34	1.38600E+01	1.44900E+01	1.26000E+00
35	1.51200E+01	1.57500E+01	1.26000E+00

Table 11. (continued)

Interval boundary No.	Distance (cm)	Internal midpoint (cm)	Internal width (cm)
36	1.63800E+01	1.65375E+01	3.14987E-01
37	1.99650E+01	1.68525E+01	3.15002E-01
38	1.70100E+01	1.71675E+01	3.15002E-01
39	1.73250E+01	1.74825E+01	3.15002E-01
40	1.76400E+01	1.77975E+01	3.15002E-01
41	1.79550E+01	1.81125E+01	3.15002E-01
42	1.82700E+01	1.84275E+01	3.15002E-01
43	1.85850E+01	1.87425E+01	3.15002E-01
44	1.89000E+01	1.90786E+01	3.57239E-01
45	1.92572E+01	1.94359E+01	3.57254E-01
46	1.96145E+01	1.97931E+01	3.57254E-01
47	1.99717E+01	2.01504E+01	3.57254E-01
48	2.03290E+01	2.05076E+01	3.57239E-01
49	2.06862E+01	2.08649E+01	3.57254E-01
50	2.10435E+01	2.12221E+01	3.57254E-01
51	2.14007E+01	2.15794E+01	3.57254E-01
52	1.75800E+01	2.19398E+01	3.63663E-01
53	2.21217E+01	2.23035E+01	3.63663E-01
54	2.24853E+01	2.26671E+01	3.63663E-01
55	2.28490E+01	2.30308E+01	3.63663E-01
56	2.32126E+01	2.33945E+01	3.63663E-01
57	2.35763E+01	2.37581E+01	3.63678E-01
58	2.39400E+01	2.45700E+01	1.25999E+00
59	2.52000E+01	2.58300E+01	1.25999E+00
60	2.64600E+01	2.70900E+01	1.25999E+00
61	2.77200E+01	2.83500E+01	1.26001E+00
62	2.89800E+01	2.96100E+01	1.25999E+00
63	3.02400E+01	3.08700E+01	1.25999E+00
64	3.15000E+01	3.21300E+01	1.26001E+00
65	3.27600E+01	3.33900E+01	1.25999E+00
66	3.40200E+01	3.46500E+01	1.26001E+00
67	3.52800E+01	3.54900E+01	4.19998E-01
68	3.57000E+01	3.59100E+01	4.19998E-01
69	3.61200E+01	3.63300E+01	4.19998E-01
70	3.65400E+01	3.66660E+01	2.51999E-01

Table 11. (continued)

Interval boundary No.	Distance (cm)	Internal midpoint (cm)	Internal width (cm)
71	3.67920E+01	3.69180E+01	2.51999E-01
72	3.70440E+01	3.71700E+01	2.51999E+01
73	3.72960E+01	3.74220E+01	2.51999E-01
74	3.75480E+01	3.76740E+01	2.52014E-01
75	3.78000E+01	3.79786E+01	3.57239E-01
76	3.81572E+01	3.83358E+01	3.57254E-01
77	3.85145E+01	3.86931E+01	3.57254E-01
78	3.88717E+01	3.90504E+01	3.57254E-01
79	3.92990E+01	3.94076E+01	3.57239E-01
80	3.95862E+01	3.97648E+01	3.57254E-01
81	3.99435E+01	4.01221E+01	3.57254E-01
82	4.03007E+01	4.04794E+01	3.57254E-01
83	4.06580E+01	4.08398E+01	3.63663E-01
84	4.10217E+01	4.12035E+01	3.63663E-01
85	4.13853E+01	4.15671E+01	3.63663E-01
86	4.17490E+01	4.19308E+01	3.63663E-01
87	4.21126E+01	4.22945E+01	3.63663E-01
88	4.24763E+01	4.26581E+01	3.63678E-01
89	4.28400E+01	4.33818E+01	1.08360E+00
90	4.39236E+01	4.44654E+01	1.08360E+00
91	4.50072E+01	4.55490E+01	1.08360E+00
92	4.60908E+01	4.66326E+01	1.08360E+00
93	4.71744E+01	4.77162E+01	1.08360E+00
94	4.82580E+01	4.87557E+01	9.95392E-01
95	4.92534E+01	4.97511E+01	9.95392E-01
96	5.02488E+01	5.07465E+01	9.95407E-01
97	5.12442E+01	5.17419E+01	9.95392E-01
98	5.22396E+01	5.27373E+01	9.95407E-01
99	5.32350E+01	5.37075E+01	9.44992E-01
100	5.41800E+01	5.46525E+01	9.44992E-01
101	5.51200E+01	5.55975E+01	9.45007E-01
102	5.60700E+01	5.65425E+01	9.44992E-01
103	5.70150E+01	5.74875E+01	9.45007E-01
104	5.79600E+01		

Note: I-mesh intervals = J-Mesh intervals

Table 12. 10-group axial leakage approximation

	$[DB^2]_{z,g}$ (cm^{-1})			
	Zones			
Group	1,15-18,20 (H_2O)	3-10 (3.3% fuel + pyrex)	11-13,21-26 (4.0% fuel)	2,14,19 (SS-304)
1	5.3842E-03	5.5355E-03	5.2252E-03	4.1736E-03
2	2.5306E-03	2.7914E-03	2.7841E-03	4.1258E-03
3	1.4246E-03	1.6644E-03	1.6723E-03	2.3227E-03
4	1.0034E-03	1.2249E-03	1.1874E-03	1.1737E-03
5	9.2890E-04	1.1802E-03	1.1354E-03	9.3560E-04
6	9.3100E-04	1.1878E-03	1.1053E-03	7.6870E-04
7	9.2420E-04	1.1525E-03	1.0787E-03	8.9610E-04
8	8.8470E-04	1.1363E-03	1.0689E-03	8.7890E-04
9	8.0010E-04	1.1063E-03	1.0456E-03	8.5200E-04
10	3.1770E-04	5.6010E-04	5.4410E-04	7.5860E-04

Table 13. Fission spectrum used in the 2-D VENUS calculation

Group	Fission spectrum*
1	4.43542E-01
2	5.01062E-01
3	5.31616E-02
4	2.14101E-03
5	1.00746E-04
6	5.37419E-06
7	2.53420E-07
8	1.27239E-08
9	8.80453E-10
10	2.29249E-10

*These values are based on ENDF/B-V data.

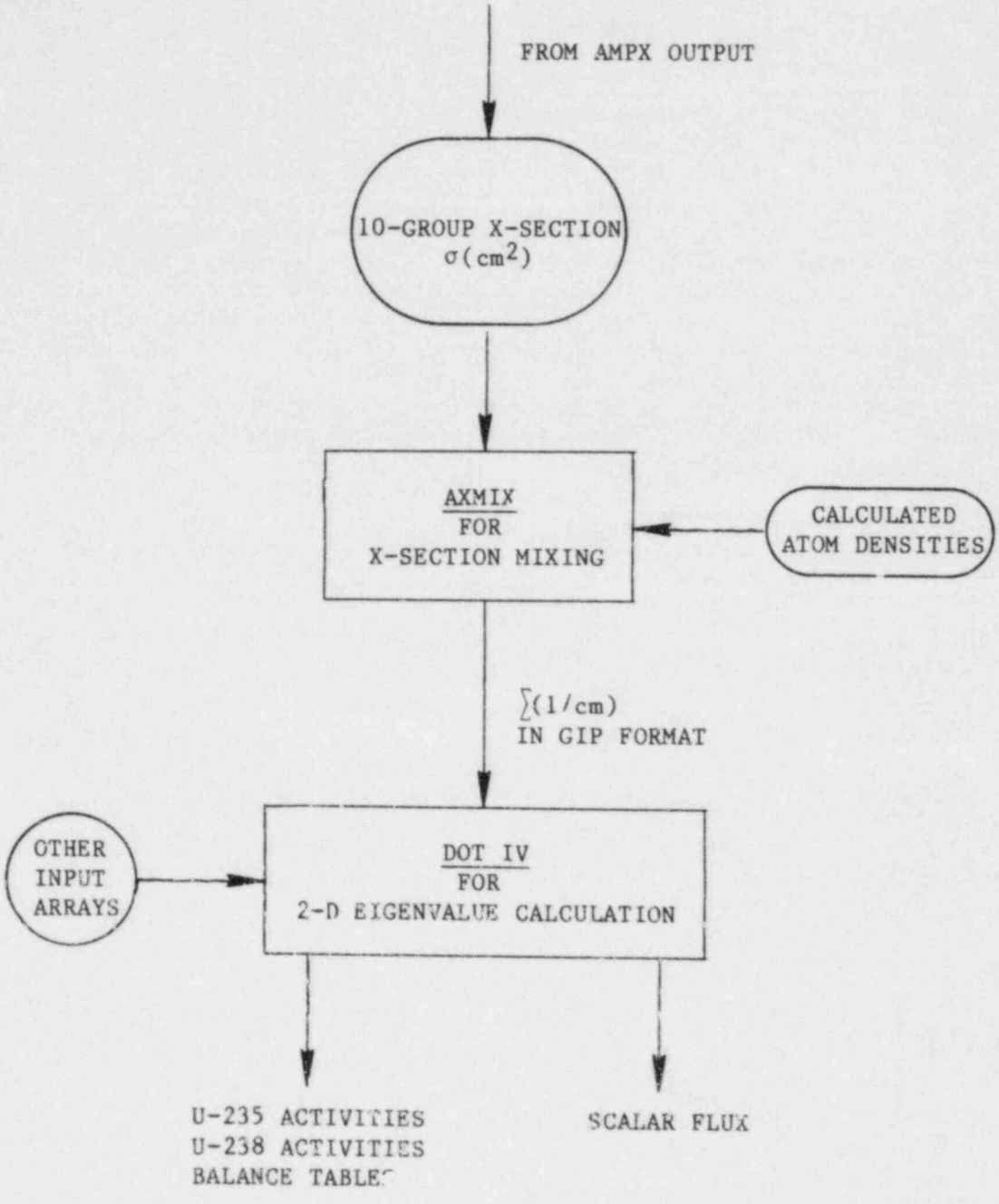

Fig. 11. Flow chart of DOT IV input and output.

5.2 FIXED-SOURCE CALCULATION

In order to accurately estimate the activities for the Np-237 fission-chamber results, a 56-group (instead of the 10-group) neutron cross section library was used. The fission cross section for Np-237 has a relatively high-energy threshold, and the 10-group structure does not adequately represent the high-energy range. Thus, a new transport calculation which used the 56-group ELXSIR[14] cross-section library, and a fixed-fission source was performed. The fixed source used in the calculations corresponded to the VENUS core fission source obtained from the 10-group eigenvalue calculation. The same mesh was used in the 56-group results. However, only one boundary zone was used to represent the outer 4.0% fuel region (as opposed to seven zones in the 10-group calculation), because the effects of variations in the thermal cross sections are insignificant in this calculation. The flow chart of the 56-group DOT IV calculation is shown in Fig. 12.

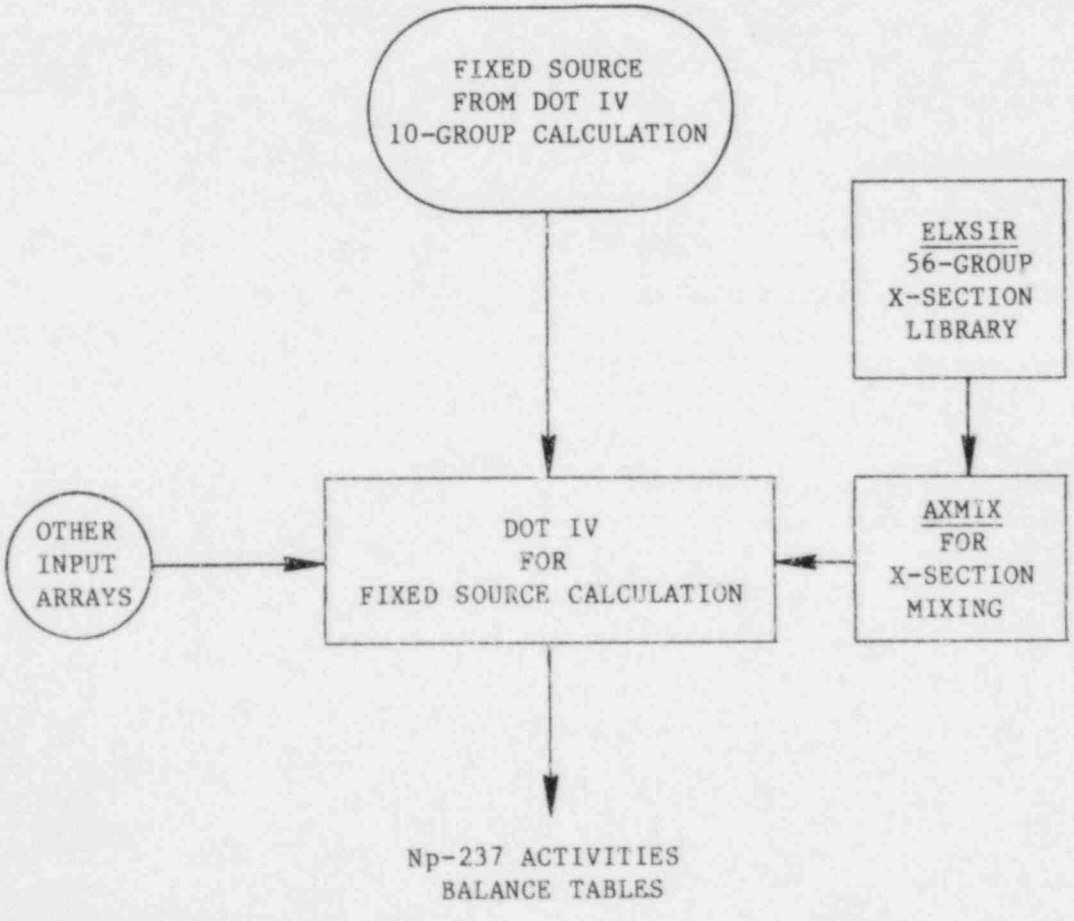

Fig. 12. Flow chart of the 56-group DOT IV calculation.

6. RESULTS

6.1 ONE-DIMENSIONAL CALCULATIONS

While performing the 218-group, one-dimensional transport calculations, it was observed that the thermal neutron spectrum hardens around the periphery of the core-baffle* interface. This behavior has an effect on the collapsed thermal cross-section values used in the two-dimensional calculations. It was realized from the outset that a transition would occur in the region near the baffle from an asympotic core spectrum to one representative of a thermal spectrum in iron. Prior to the present calculations, a transition zone of 2.52 cm was used to collapse "boundary-weight" cross sections. However, it was later realized that a single transition zone of 2.52 cm is too coarse, due to the rapid changes in the thermal spectrum within the last 2 cm of the core boundary. It became necessary that more zones be used in the core-baffle region to account properly for the thermal spectrum changes. As a result, a total of seven zones was used for the one-dimensional calculations to obtain a separately weighted set of collapsed cross sections at approximately every one-quarter centimeter in the core-baffle region of 2.52 cm. The effect of this zone-weighting procedure on the collapsed U-235 thermal fission cross section is shown in Table 14. Notice the significant variation of the cross sections in the core-baffle region of 2.52 cm. Also in the two-dimensional calculation, seven zones with different cross-section weightings were used for the core-baffle region.

6.2 TWO-DIMENSIONAL CALCULATIONS

The effective multiplication factor for the two-dimensional X-Y calculations was determined to be $k_{eff} = 0.996$. This value was underpredicted by about one half of one percent. The low value of k_{eff} is consistent with other LWR lattice studies which show that the ENDF/B-IV cross sections tend to underestimate the eigenvalue due to excessive U-238 capture estimates.

A set of 10-group fluxes was obtained from the eigenvalue calculation. Three-dimensional plots of the thermal flux (i.e., group 10 with $E < 0.650$ eV), and the fast flux of group 1 (with $E > 1.850$ MeV), as a function of position for the VENUS model are shown in Figs. 13 and 14, respectively. The plot of Fig. 13 shows that the thermal flux has its highest peak at the core center in the water hole. This is due to the fact that many fission neutrons are thermalized in the water hole.

*This discussion is confined to the outer baffle-core region, since this is the area that contributes most to RPV fluence.

Table 14. Variation of U-235 thermal fission cross section*

Distance from outer baffle (cm)	Description	U-235 group 10/10 fission cross section (barns)
0.252	Outer 4.0% fuel	250.35
0.504	Outer 4.0% fuel	255.79
0.756	Outer 4.0% fuel	259.64
1.008	Outer 4.0% fuel	262.40
1.260	Outer 4.0% fuel	264.55
1.512	Outer 4.0% fuel	266.28
2.520	Outer 4.0% fuel	269.41
2.52-18.90	Inner 4.0% fuel	278.80

*These are collapsed values and are applicable to the 4.0% fuel region only.

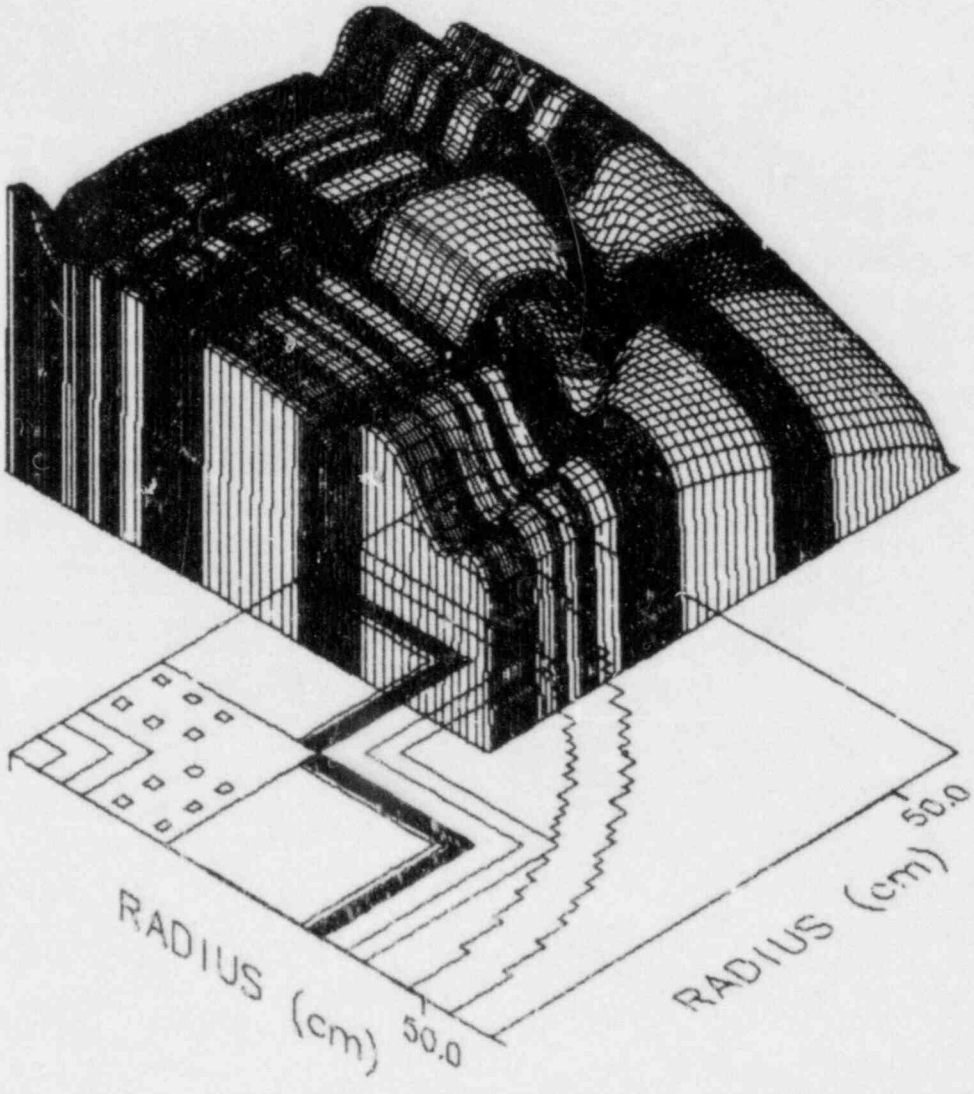

Fig. 13. Thermal flux of group 10 for the VENUS model.

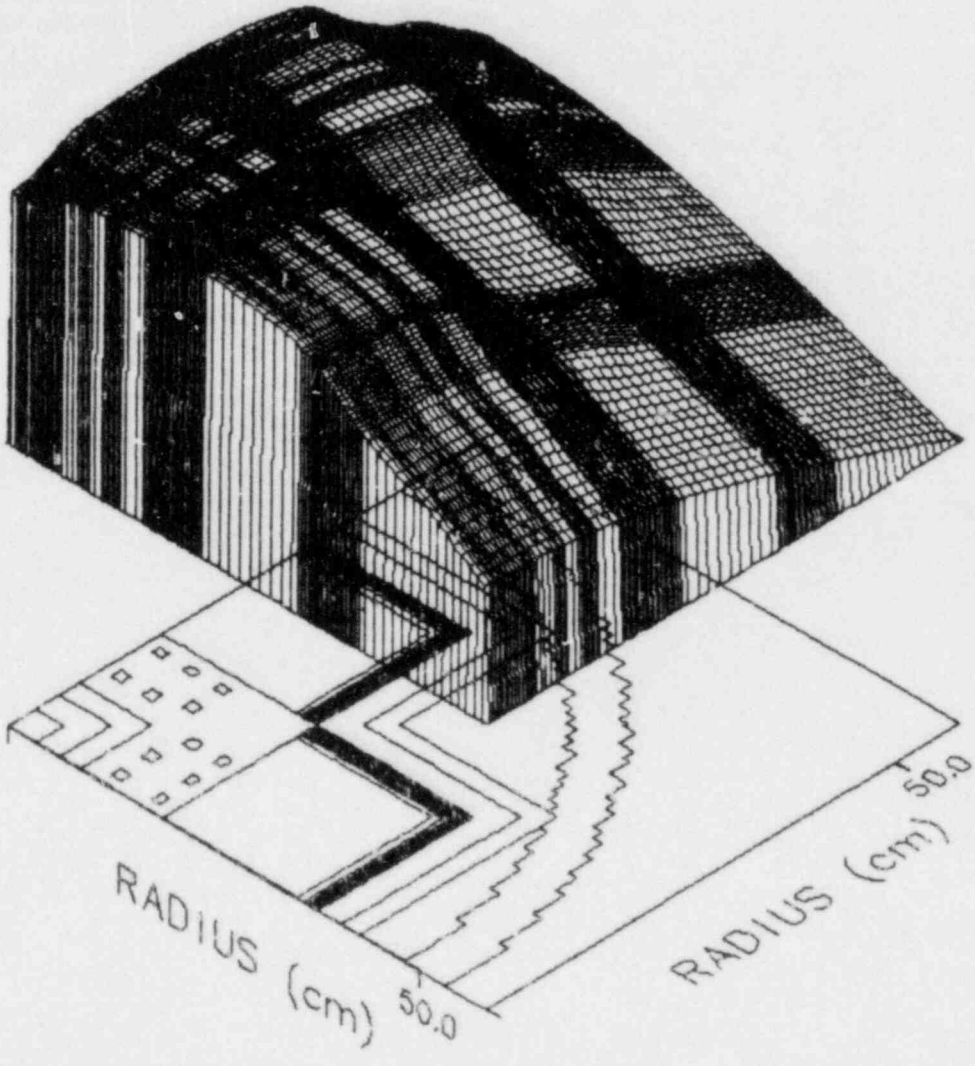

Fig. 14. Fast flux of group 1 for the VENUS model.

Other peaks can be observed in the water reflector region and the water pool. Notice the depression of thermal flux in the steel baffles and barrel. The biggest flux depression is in the steel barrel, and this is because the flux sees more iron in the barrel, relative to the baffles. On the other hand, the plot of Fig. 14 indicates that the fast flux peaks around the fuel cells area, and that there is less depression in iron. Notice the flattening of the fast flux peak, which is due to the power flattening by the pyrex cells. It can also be seen that the number of fast neutrons decreases towards the core edges, and it reaches a minimum in the water pool.

On the basis of the 10-group fluxes, the total space-dependent fission rate throughout the core was calculated, accounting for both U-235 and U-238 fissions. The U-235 fission rate is due to thermal and epithermal neutrons, and the U-238 fission rate is due to fast neutrons. The fission distribution was normalized to obtain a relative pin-by-pin power distribution as shown in Fig. 15. These calculations used the detailed, spatially weighted cross sections near the core-baffle interface.

Fission-chamber results for the 10-group, X-Y calculation (i.e., U-235 activity) and the 56-group calculation (i.e., Np-237 activity) were obtained at selected locations in the steel baffle and in the steel barrel of the VENUS core. The U-235 activity is sensitive to low-energy neutrons; and the Np-237 activity, which has a threshold of about 100 KeV, is for high-energy neutrons. The locations are shown in Fig. 16. The fission-rate results and the corresponding normalized values are given in Table 15.

6.3 EXPERIMENTAL MEASUREMENTS[15]

By using gamma scans of various fuel pins removed from the core, Mol was able to deduce the relative fission rates in the VENUS core. Fig. 17 shows the normalized values of the experimentally measured power distribution. Notice that some of the values were obtained by interpolation.

The U-235 and Np-237 fission-chamber measurements for locations shown in Fig. 16 are given in Table 16.

Unit: Total fission/sec./cell

NORMALIZATION (per unit height)

Core average fission rate = 1 fiss./sec./cell

Total 1/8 core = 319 fiss./sec.

Total core = 2552 fiss./sec.

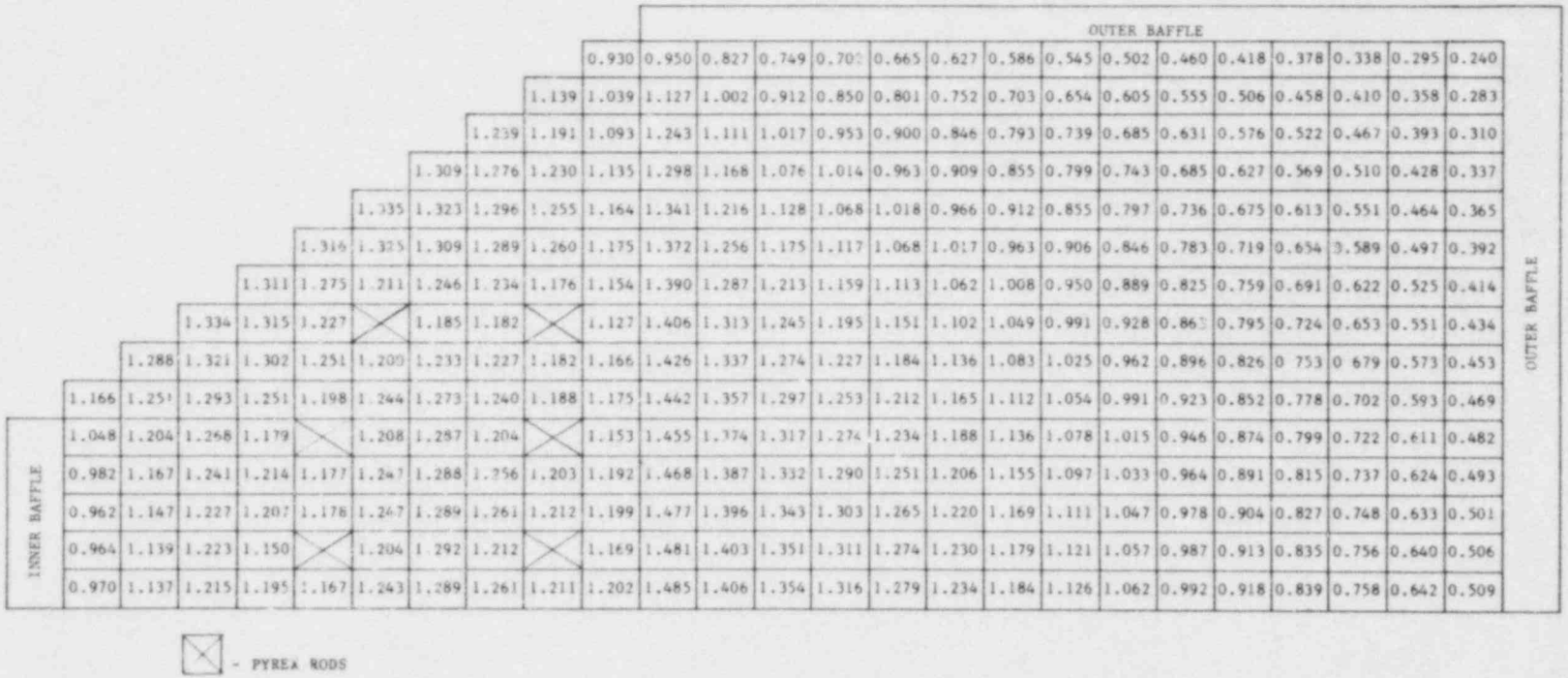

Fig. 15. Calculated radial power distribution for 1/8 of the VENUS core.

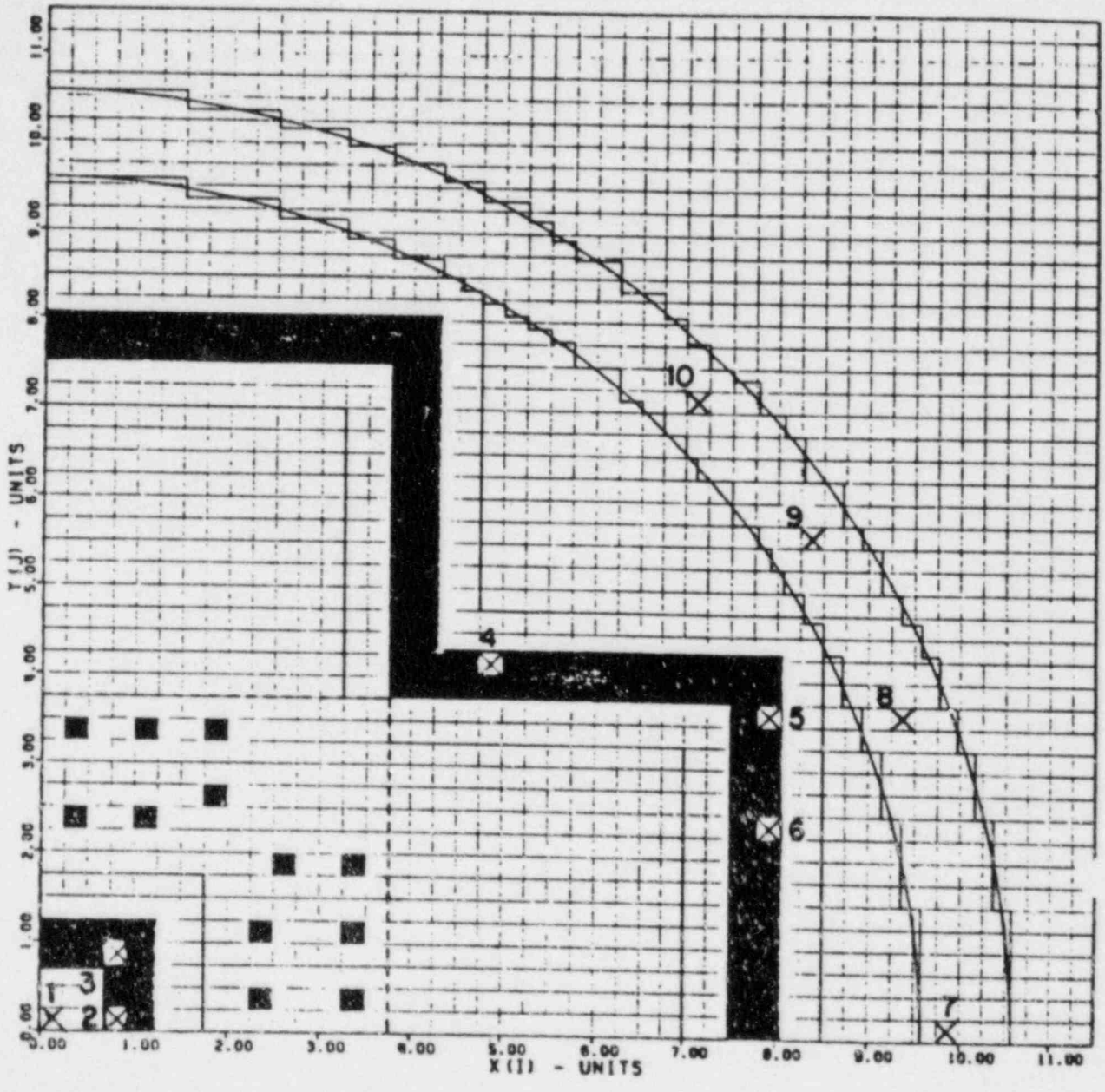

Fig. 16. Fission chamber locations in the VENUS model (Scale: 1 unit = 4 pin pitches = 5.04 cm).

Table 15. Results of fission chamber calculations

No.	Position†	X(I) (cm)	Y(J) (cm)	U-235 fission rate		Np-237 fission rate	
				Calculated value	Normalized* value	Calculated value	Normalized* value
1	WH(45°)	0.63	0.63	11.1800	7.2597	6.695E-03	0.6205
2	IB(8.13°)	4.41	0.63	1.5400	1.0	1.079E-02	1.0
3	IB(45°)	4.41	4.41	0.9660	0.627[illegible]	1.275E-02	1.1816
4	OB(40.24°)	24.57	20.79	0.7540	0.4896	6.380E-03	1.5913
5	OB(24.72°)	39.69	18.27	0.2730	0.1773	1.985E-03	0.1840
6	OB(16.78°)	39.69	11.97	0.4010	0.2604	3.315E-03	0.3072
7	B(0.725°)	49.77	0.63	0.1560	0.1013	5.030E-04	0.0466
8	B(21.14°)	47.25	18.25	0.0865	0.0562	4.600E-04	0.0426
9	B(33.9°)	42.21	28.35	0.0586	0.0380	3.250E-04	0.0301
10	B(45°)	35.91	35.91	0.0538	0.0349	2.256E-04	0.0209

†WH = water hole, IB = inner baffle, OB = outer baffle, B = barrel.
*Normalized to 1.0 at IB(8.13°) position.

Note: Underlined values are experimental data. Other values are interpolated.
Unit: Total fiss./sec./cell
NORMALIZATION (per unit height)
Core average fission rate = 1 fiss./sec./cell
Total 1/8 Core = 319 fiss./sec.
Total core = 2552 fiss./sec.

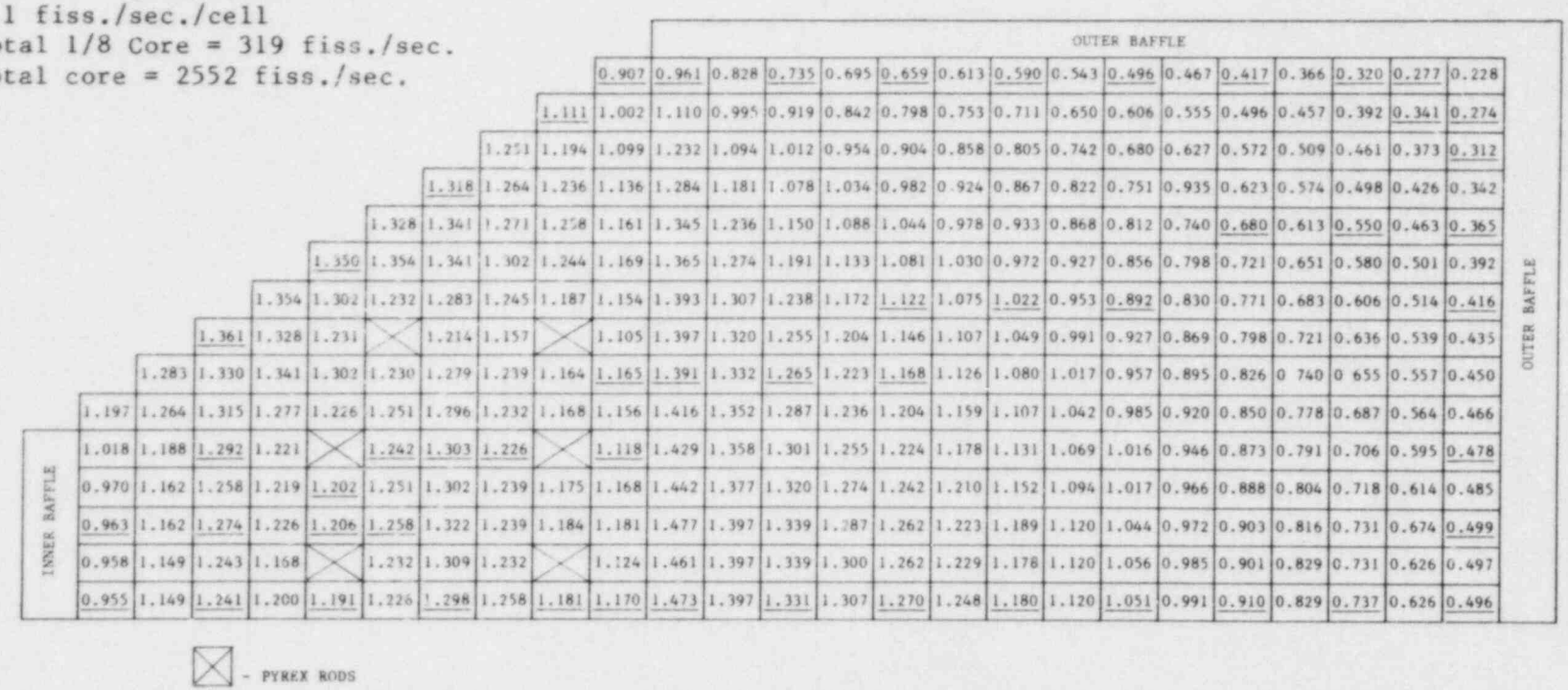

Fig. 17. Measured radial power distribution for the VENUS core.

Table 16. Results of fission chamber calculations

No.	Position†	X(I) (cm)	Y(J) (cm)	U-235 fission rate		Np-237 fission rate	
				Measured value	Normalized* value	Measured value	Normalized* value
1	WH(45°)	0.63	0.63	-	-	1.550E+09	0.6568
2	IB(8.13°)	4.41	0.63	4.960E-13	1.0	2.360E+09	1.0
3	IB(45°)	4.41	4.41	-	-	2.800E+09	1.1864
4	OB(40.24°)	24.57	20.79	2.520E-13	0.5081	1.410E+09	0.5974
5	OB(24.72°)	39.69	18.27	-	-	4.240E+08	0.1797
6	OB(16.78°)	39.69	11.97	1.290E-13	0.2601	7.380E+09	0.3127
7	B(0.725°)	49.77	0.63	-	-	1.180E+08	0.0500
8	B(21.14°)	47.25	18.25	2.630E-14	0.0530	1.090E+08	0.0462
9	B(33.9°)	42.21	28.35	-	-	7.330E+07	0.0310
10	B(45°)	35.91	35.91	1.460E-14	0.0294	5.510E+07	0.0233

†WH = water hole, IB = inner baffle, OB = outer baffle, B = barrel.
*Normalized to 1.0 at IB(8.13°) position.

7. COMPARISON OF CALCULATION TO MEASUREMENTS AND DISCUSSION OF RESULTS

7.1 COMPARISON OF CALCULATIONAL AND EXPERIMENTAL MEASUREMENTS

Relative power distribution

A comparison of the calculated and measured relative power distribution of the VENUS model is shown in Fig. 18. The average agreement between calculation and experiment is within 3% error, with an uncertainty of about 1.5% in the measurements. The worst agreement has an error of 6.5%, and it occurs in a cell near the baffle corner. Disagreements of up to 3% can also be found at locations near the pyrex rods. The error introduced into the computed RPV fluence by these source discrepancies should be on the order of 5% or less. Agreement could be improved, perhaps, by adding more zones in the core-baffle interface region.

Fission chamber responses

The ratio of the fission chamber response calculations-to-experimental measurements are given in Table 17. The corresponding fission chamber locations can be found in Fig. 16. Both the calculated and measured values are normalized so that the U-235 and Np-237 fission rate at point 2 in the inner baffle is equal to unity. It can be seen that the relative C/E values in the baffles are very close to unity, indicating good agreement. The worst agreement is in the barrel, and this can be attributed to the fact that a rectangular approximation was used for the circular barrel. Nevertheless, the average agreement between calculation and experiment is good, considering the fact that the U-235 and Np-237 dosimeters were located in the excore areas, for which the R-θ calculational model is best suited.

7.2 DISCUSSION OF RESULTS

The analysis of the fission rate calculation shows that the fission source peaks around the 3.3% and 4.0% fuel boundary region, with the 4.0% fuel contributing the most (about 64%) to the total fission rate, and the 3.3% fuel contributing the highest average peak values. Results also indicate that the fission source approaches a minimum at the core-outer baffle interface, with the ultimate minimum at the steel baffle corner. If there were no outer baffle at the core boundary, the neutrons that thermalize in the water reflector would have contributed significantly to the fission source at the fuel-reflector region to establish a local maximum of neutrons. The fact that we have a local minimum suggests that the steel baffle is consuming the neutrons which thermalize in the water reflector before they can re-enter the core. The result is that the RPV fluence is greatly reduced by the presence of the outer baffle.

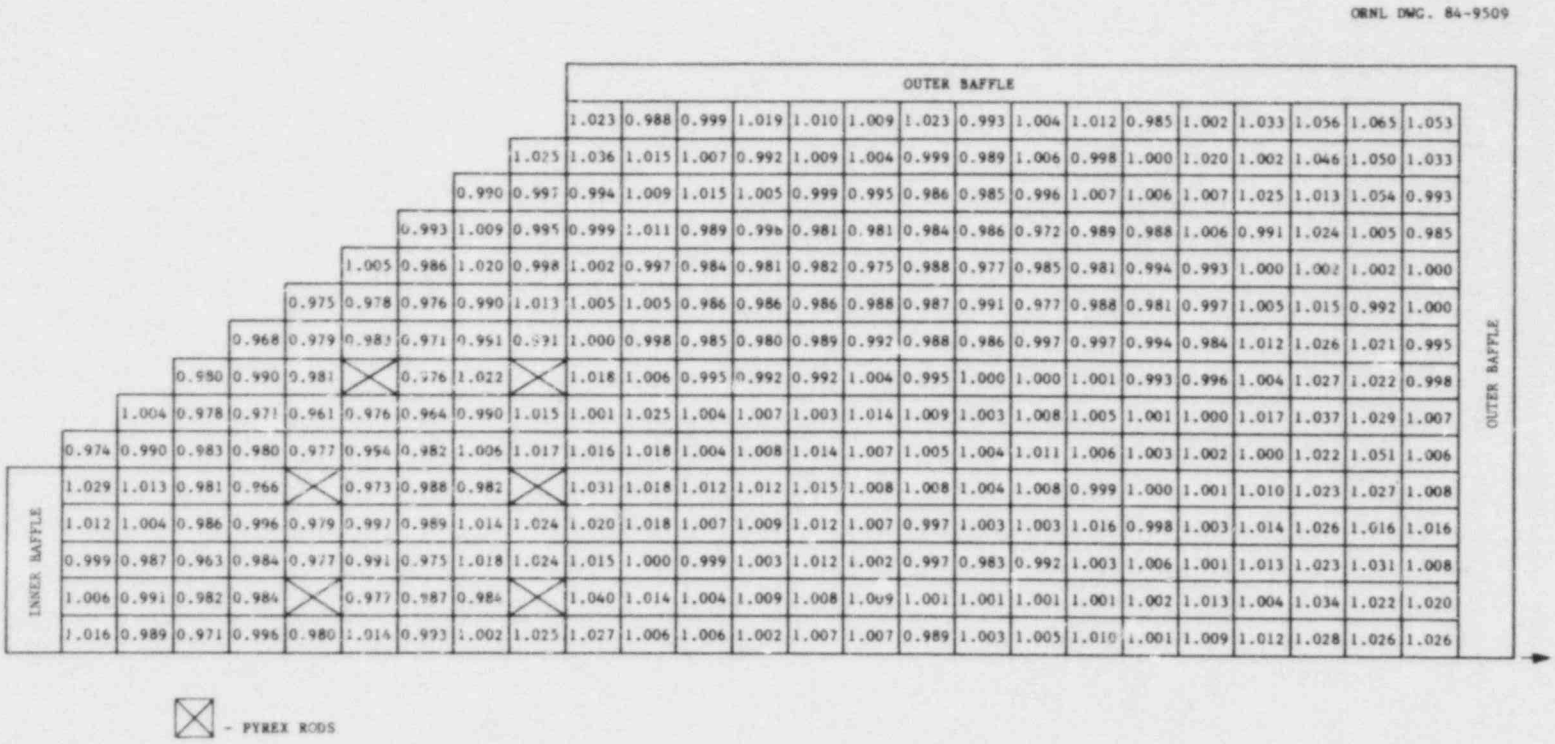

Fig. 18. Comparison of calculated and measured relative power distribution.

Table 17. Comparison of fission chamber calculations with experiment

No.	Position†	X(I) (cm)	Y(J) (cm)	U-235 fission rate			Np-237 fission rate		
				Calc.	Expt.	C/E	Calc.	Expt.	C/E
1	WH(45°)	0.63	0.63	7.2597	-	-	0.6205	0.6568	0.9447
2	IB(8.13°)	4.41	0.63	1.0	1.0	1.0	1.0	1.0	1.0
3	IB(45°)	4.41	4.41	0.6273	-	-	1.1816	1.1864	0.9959
4	OB(40.24°)	24.57	20.79	0.4896	0.5081	0.9636	0.5913	0.5974	0.9898
5	OB(24.72°)	39.69	18.27	0.1773	-	-	0.1840	0.1797	1.0239
6	OB(16.78°)	39.69	11.97	0.2604	0.2601	1.0011	0.3072	0.3127	0.9824
7	B(0.725°)	49.77	0.63	0.1013	-	-	0.0466	0.0500	0.9320
8	B(21.14°)	47.25	18.25	0.0562	0.0530	1.0604	0.0426	0.0462	0.9221
9	B(33.9°)	42.21	28.35	0.0380	-	-	0.0301	0.0310	0.9710
10	B(45°)	35.91	35.91	0.0349	0.0294	1.1871	0.0209	0.0233	0.8970

†WH = water hole, IB = inner baffle, OB = outer baffle, B = barrel.

While the fission rate in the last row of the fuel cells approaches a minimum at the outer baffle corner, the fission rate of the fuel cells along the inner baffle decreases to a minimum, and then increases to a maximum at the corner. This behavior is a duplication of the thermal flux distribution in the region and it is probably due to a combination of the slowing-down neutrons in the core and the thermal neutrons leaking from from the water hole. It should be mentioned that the core neutron source distribution measurements from Mol do not reflect this phenomenon, probably because most of the measurements in the region were obtained by interpolation.

It can also be observed that the flux around the pyrex region is depressed, resulting in an appreciable flattening of the core power distribution. The result is that the power distribution spreads to the core edges in order to facilitate accurate ex-core measurements.

The normalized fission chamber results show that the calculated U-235 values are slightly higher than the normalized measured values, while the calculated Np-237 values are slightly lower than the normalized measured values. It can also be seen that the Np-237 disagreement increases with more iron penetration, particularly in the steel barrel. The low C/E values for Np-237 is probably due to the ENDF/B-IV iron inelastic cross sections which are thought to be too large, thereby resulting in an overprediction of attenuation of high-energy neutrons through the baffles and barrel.

In addition to those obtained from the 10-group calculations, the U-235 fission rate results obtained from the 56-group calculation were also compared to the measured U-235 fission chamber responses. It was found that the errors are of higher magnitude relative to the errors from the U-235 fission chamber results of the 10-group calculation (see Table 18). This is because the ELXSIR 56-group, cross-section library, which has a "generic" thermal group cross section and therefore, does not adequately represent the thermal spectrum in the various zones of the VENUS configuration. Recall that the thermal cross section in the 10-group set was weighted specifically for the VENUS configuration.

Measurements in the inner baffle can be related to measurements in the outer baffle since both baffles are bounded by water which thermalize the fission neutrons. In essence, the water hole provides a reference field for checking the validity of the techniques used for the study of the neutron propagation across the baffle and outside the core. Spectrometer measurements have been made in this region, and will be examined in a later study.

The fact that the overall calculation is in good agreement with experimental measurements establishes that uncertainties in the core source calculation are tolerable in the computation of the RPV fluence.

Table 18. U-235 fission chamber C/E values for 10-group and 56-group calculations

No.	Position	X(I) (cm)	Y(J) (cm)	C/E values for U-235 responses	
				10-group calc.	56-group calc.
1	WH(45°)	0.63	0.63	-	-
2	IB(8.13°)	4.41	0.63	1.0	1.0
3	IB(45°)	4.41	4.41	-	-
4	OB(40.24°)	24.57	20.79	0.9636	1.1543
5	OB(24.72°)	39.69	18.27	-	-
6	OB(16.78°)	39.69	11.97	1.0011	1.1888
7	B(0.725°)	49.77	0.63	-	-
8	B(21.14°)	47.25	18.25	1.0604	0.7849
9	B(33.9°)	42.21	28.35	-	-
10	B(45°)	35.91	35.91	1.1871	0.7347

8. CONCLUSIONS AND RECOMMENDATIONS

8.1 CONCLUSIONS

Few group cross sections were generated for the VENUS configuration and shown to give better agreement with experiment for thermal responses like U-235 fission, than the ELXSIR (or VITAMIN-C) cross-section library. The critical eigenvalue computed with these cross sections was 0.996.

An important discovery of this report is that the thermal flux changes rapidly as a function of position in the outer baffle-core interface region, which is the most important region for contributing to RPV fluence. It was discovered that the neutron source in the core-baffle region can be accurately calculated by using several separately weighted cross sections at the appropriate points in the region. An increased number of separately weighted cross sections corresponds to a greater degree of accuracy; however, this significantly increases the calculational complexity and may not be practical for analysis of power reactors. A total of seven separately weighted cross sections were used in the core-baffle interface region of the VENUS model.

Comparison of calculation with measured relative power distribution indicates that the shape of the neutron source can be computed within an accuracy of 3% error at most locations near the important core-baffle region, and an average agreement of about 3% error for the whole in-core area. At the corner location of the core (i.e., the point closest to the barrel), however, the agreement was about 6%. Also, the compared values of normalized, calculated and measured U-235 and Np-237 fission rates in the ex-core region are in good agreement. The worst agreement is in the circular barrel, which was approximated in the X-Y model as a rectangular geometry. It is believed that a better accuracy for the ex-core calculation can be obtained with an R-θ model of the VENUS configuration.

In conclusion, the space-dependent neutron fission rate in the VENUS core, particularly at the core periphery can be accurately calculated with discrete ordinates transport theory. A high degree of accuracy can be obtained by using a detailed set of space-dependent cross-section weightings in the important outer baffle-core interface region. It is estimated the discrepancies in the computed neutron source will introduce no more than a 5% error in calculated dosimeter reaction rates for this configuration.

8.2 RECOMMENDATIONS FOR FUTURE WORK

It is recommended that an R-θ model be used in the ex-core calculation to be performed in Phase II of the VENUS analysis. This is expected to include the surveillance dosimeter measurements and the RPV fluence calculation that is commonly used in assessing RPV embrittlement. Mol has recently obtained neutron spectrum measurements with proton recoil spectrometers, and these measurements should be compared with the calculated 56-group spectrum.

In addition to the neutronic studies, the gamma flux distribution will be calculated in Phase III of the analysis, with a view of providing estimates of the gamma doses and heating rates at several locations, and the ratio of gamma dose rate to thermal neutron flux.

Finally, the VENUS benchmark can be extended to validate the two-group diffusion theory, which is the standard core analysis method used by utilities. This will provide a true measure of the effectiveness of the diffusion theory method, relative to the discrete ordinates transport theory method.

9. REFERENCES

1. T. U. Marston et al., "A Report on the EPRI Pressurized Thermal Shock Program," Presented at the 10th Water Reactor Safety Research Information Meeting, Gaithersburg, MD, October 15, 1982.

2. R. D. Cheverton, "A Brief Account of the Effect of Overcooling Accidents on the Integrity of PWR Pressure Vessel," Proc. of the 4th ASTM-EURATOM Symposium on Reactor Dosimetry, NUREG/CP-0029, NRC, Washington, DC, Vol. 2, pp. 1061-1070, July 1982.

3 R. Smock, "Thinking the Unthinkable: NRC's Guidelines Aimed at Preventing Pressure Vessel Failure," Electric Light and Power, December 1982.

4. G. Minsart, Design Study of the Core Loading for the VENUS PWR Pressure Vessel Benchmark Facility, CEN/SCK, Mol, Report 380/82-27, October 5, 1982.

5. L. Leenders, "Definitions of Qualification of the Materials Used in the VENUS Configuration," Correspondence from CEN/SCK in Mol, Belgium to Oak Ridge National Laboratory, 1983.

6. W. E. Ford, III, C. C. Webster, and R. M. Westfall, A 218-Group Neutron Cross-Section Library in the AMPX Master Interface Format for Criticality Safety Studies, ORNL/CSD/TM-4, Oak Ridge National Laboratory, Oak Ridge, TN, July 1976.

7. L. W. Nordheim, "Theory of Resonance Absorption," Proc. of Symposia in Applied Mathematics, Vol. XI, P. 58, G. Birkhoff and E. P. Wigner, Eds., American Mathematics Society, 1961.

8. R. M. Westfall, L. M. Petrie, N. M. Greene, and J. L. Lucius, NITAWL-S: Scale System Module for Performing Resonance Shielding and Working Library Production, NUREG/CR-0200, Vols. 1-3, ORNL/NUREG/CSD-2/R1, NRC, Washington, DC, July 1982.

9. L. M. Petrie, N. M. Greene, J. L. Lucius, and J. E. White, NITAWL: AMPX Module for Resonance Self-Shielding and Working Library Production, PSR-63/AMPX-II, November 1978.

10. L. M. Petrie and N. M. Greene, XSDRNPM-S: A One-Dimensional Discretes Ordinates Code for Transport Analysis, NUREG/CR-0200, Vol. 2, Section F3, ORNL/NUREG/CSD-2/V3/R1, NRC Washington, DC, July 1982.

11. N. M. Greene et al., "AMPX: A Modular System for Multigroup Cross-Section Generation and Manipulation," A Review of Multigroup Nuclear Cross-Section Processing, Proceedings of a Seminar-Workshop, Oak Ridge, TN, March 14-16, 1978.

12. W. A. Rhoades and R. L. Childs, An Updated Version of the DOT IV One- and Two-Dimensional Neutron/Photon Transport Code, ORNL-5851, Oak Ridge National Laboratory, Oak Ridge, TN, April 1982.

13. W. E. Ford, III et al., CSRL-V: Processed ENDF/B-V 227-Neutron-Group and Pointwise Cross-Section Libraries for Criticality Safety, Reactor and Shielding Studies, NUREG/CR-2306, ORNL/CSD/TM-160, NRC, Washington, DC, June 1982.

14. M. L. Williams, R. E. Maerker, W. E. Ford, III, and C. C. Webster, The ELXSIR Cross-Section Library for LWR Pressure Vessel Irradiation Studies, Oak Ridge National Laboratory, Oak Ridge, TN, July 1983.

15. A. Fabry et al., "Experimental Results," Correspondence from CEN/SCK in Mol, Belgium to Oak Ridge National Laboratory, Oak Ridge, TN, 1983/84.

16. J. R. Lamarsh, Introduction to Nuclear Reactor Theory, Addison-Wesley Publishing Co., pp. 370-400, 1966.

17. A. F. Henry, Nuclear Reactor Analysis, The MIT Press, pp. 66-80, 84-87, 200-253, 333-343, 1975.

18. G. C. Haynes, The AXMIX Program for Cross-Section Mixing and Library Arrangement, ORNL/TM-5295, Oak Ridge National Laboratory, Oak Ridge, TN, December 1974.

19. A. Fabry et al., "Improvement of LWR Pressure Vessel Steel Embrittlement Surveillance: Progress Report on Belgian Activities in Cooperation with the USNRC and other R&D Programs," Proc. of the 4th ASTM-EURATOM Symposium on Reactor Dosimetry, Gaithersburg, MD, March 22-26, 1982, NUREG/CP-0029, NRC, Washington, DC, Vol. 1, pp. 45-77, July 1982.

20. W. N. McElroy et al., "Surveillance Dosimetry of Operating Power Plant," Proc. of the 4th ASTM-EURATOM Symposium on Reactor Dosimetry, Gaithersburg, MD, March 22-26, 1982, NUREG/CP-0029, NRC, Washington, DC, Vol. 1, pp. 3-43, July 1982.

21. D. L. Phung and W. B. Cottrell, "Analyzing Precursors to Severe Themal Shock," Nuclear Engineering International, February 1983.

22. P. N. Randall, "Status of Regulatory Demands in the U.S. on the Application of Pressure Vessel Dosimetry," Proc. of the 4th ASTM-EURATOM Symposium on Reactor Dosimetry, Gaithersburg, MD, March 22-26, 1982, NUREG/CP-0029, NRC, Washington, DC, Vol. 2, pp. 1011-1022, July 1982.

23. M. L. Williams, R. Q. Wright, and J. Barhen, Development of Improved Methods for the LWR Lattice Physics Code EPRI-CELL, ORNL/TM-8411, Oak Ridge National Laboratory, Oak Ridge, TN, July 1982.

24. W. A. Rhoades and M. B. Emmett, DOS: The Discrete Ordinates System, ORNL/TM-8362, Oak Ridge National Laboratory, Oak Ridge, TN, September 1982.

25. W. Rothenstein, "Resonance Absorption Calculations in Thermal Reactors," Progress in Nuclear Energy, Vol. 5, pp. 95-144, 1980.

26. M. L. Williams, "Correction of Multigroup Cross Sections for Resolved Resonance Interference in Mixed Absorbers," Nuclear Science and Engineering, 1983.

27. W. Rothenstein, J. Barben, E. Taviv, and M. Aminpour, "Resonance Shielding in Thermal Reactor Lattices," Ann. Nucl. Energy, Vol. 9, pp. 141-168, 1982.

28. M. L. Williams, R. E. Maerker, F. W. Stallmann, and F. B. K. Kam, "Validation of Neutron Tranport Calculations in Benchmark Facilities for Improved Vessel Fluence Estimation," Proc. of the 11th WRSR Information Meeting, Gaithersburg, MD, October 24-28, 1983, NUREG/CP-0048, Vol. 1-6, NRC, Washington, DC.

29. F. B. K. Kam, F. W. Stallmann, and M. L. Williams, "Standard Practice for Analysis and Interpretation of Physics Dosimetry Results from Test Reactors," 1984 Annual Book of ASTM Standards, Vol. 12.02, American Society for Testing and Materials, Philadelphia, PA, 1984.

30. M. L. Williams, "LSU Progress Reports from May 1983 to February 1984," Internal Report from M. L. Williams to D. G. Cacuci, 1983/84.

APPENDIX A

CALCULATIONAL PARAMETERS

A.1 ATOM DENSITIES

Using the given specifications, the atom densities of all the important nuclides in each of the materials encountered in the VENUS configuration were determined.

Table A.1. contains the atom densities for the fuel elements and Tables A.2 and A.3 correspond to the atom densities for the claddings of the 4.0% and 3.3% fuel types, respectively. The atom densities of the pyrex rod and its cladding are shown in Tables A-4 and A-5, respectively. For the baffle and the moderator, Tables A.6 and A.7 show the respective atom densities. Finally, the atom densities of the homogenized fuel cells (for the 4.0% and 3.3% fuel types) and the homogenized pyrex cell are given in Tables A.8 and A.9, respectively.

A.2 REACTOR PARAMETERS

The Dancoff factors for the 4.0% and 3.3% fuel types were calculated as C = 0.2701 and C = 0.2617, respectively.

The infinite multiplication factors obtained for the 4.0% and 3.3% fuel pins, and the pyrex are $K_\infty = 1.3142$, $K_\infty = 1.3834$, and $K_\infty = 1.2490$, respectively.

Table A.10 shows the critical radius calculated for each of the zones used in the one-dimensional calculations of the VENUS configuration. Each radius is measured from the center of the cylindrical model to the zone's outer boundary.

The critical height of the one-dimensional cylindrical model that was used in a buckling correction is H = 67.44 cm.

A.3. CALCULATION OF DIFFUSION COEFFICIENTS AND DB^2

The diffusion coefficients in the leakage terms were calculated from the expression:

$$D_{z,g} = \frac{1}{3\sum_{tr}^{z,g}} \qquad (A.1)$$

where: $D_{z,g}$ ≡ diffusion coefficient for group g in zone z

$\sum_{tr}^{z,g}$ ≡ macroscopic transport cross section for group g in zone z

$$\text{But } \sum_{tr}^{z,g} = \sum_{T}^{z,g}(P_o) - \frac{1}{3}\sum_{g\to g}^{z,g}(P_1) \qquad (A.2)$$

where: $\sum_{T}^{z,g}(P_o)$ ≡ total macroscopic cross section associated with the P-zero component

$\sum_{g\to g}^{z,g}(P_1)$ ≡ macroscopic scattering cross section associated with the P-one component

Using the above expressions, a computer program of Fig. A.1 was developed, and subsequently employed in calculating the diffusion coefficients and DB^2 values. Tables A.11 and A.12 show the diffusion coefficients determined for each zone in the 10-group and 56-group two-dimensional X-Y calculations, respectively. The corresponding DB^2 values for the 10-group and 56-group calculations can be found in Tables 11 and A.13, respectively. A buckling value of $B = 24 \times 10^{-4}$ (cm^{-2}) which was obtained from Mol, was used in the axial leakage (DB^2) calculations.

```
      DIMENSION CSØ(1ØØ,1ØØ),CSI(1ØØ,1ØØ),CS2(1ØØ,1ØØ),CS3(1ØØ,1ØØ)
      DIMENSION XS(1ØØ),SIGTR(1ØØ),D(1ØØ),DB2(1ØØ),TITLE(12)
      READ(5,1)IGM,IHM,NMIX,B2
1     FORMAT(3I1Ø,F1Ø.4)
C  DO LOOP FOR MIXTURE
      DO 1Ø K=1,NMIX
      WRITE(6,5Ø)K
5Ø    FORMAT('1',1ØX,'DIFFUSION COEF. AND DB SQ FOR MIXTURE #',1X,I3,/)
      WRITE(6,6Ø)
6Ø    FORMAT(1ØX,'GROUP',15X,'D(CM)',15X,'DBSQ(1/CM)',/)
C  READ THE CROSS SECTION WITH THE P-ZERO COMPONENT
      READ(1)
      READ(1) ((CSØ(I,J),I=1,IHM),J=1,IGM)
C  READ THE CROSS SECTION WITH THE P-ONE COMPONENT
      READ(1)
      READ(1) ((CS1(I,J),I=1,IHM),J=1,IGM)
C  READ THE CROSS SECTION WITH THE P-TWO COMPONENT
      READ(1)
      READ(1) ((CS2(I,J),I=1,IHM),J=1,IGM)
C  READ THE CROSS SECTION WITH THE P-THREE COMPONENT
      READ(1)
      READ(1) ((CS3(I,J),I=1,IHM),J=1,1GM)
C  DO LOOP FOR ENERGY GROUP
      DO 2Ø J=1,IGM
C  IDENTIFY THE POSITION PRECEEDING THE SELF SCATTER GROUP
      M=5
C  INITALIZE SUM OF SCATTERING CROSS SECTION TO ZERO
      XS(J)=Ø.Ø
C  DO LOOP FOR ADDING SELF SCATTER AND DOWN SCATTER TO SUM
      DO 3Ø I=J,IGM
      M=M+1
3Ø    XS(J)=XS(J)+CS1(M,I)
C  CALCULATE TRANSPORT CROSS SECTION FOR THE GROUP
      SIGTR(J)=CSØ(5,J)-XS(J)/3.Ø
C  CALCULATE THE DIFFUSION COEFFICIENT FOR THE GROUP
      D(J)=1.Ø/(3.Ø*SIGTR(J))
C  CALCULATE DB SQUARED
      DB2(J)=D(J)*B2
C  PRINT THE DIFFUSION COEFFICIENTS AND DB SQUARED VALUES
      WRITE(6,7Ø)J,D(J),DB2(J)
7Ø    FORMAT(11X,I3,15X,F1Ø.4,15X,F1Ø.4)
2Ø    CONTINUE
      CALL FFPUN(DB2,IGM,NMIX)
1Ø    CONTINUE
      STOP
      END
```

NOTE: IGM = No. of energy groups
IHM = Table length
NMIX = No. of mixture
B2 = B^2 value

Fig. A.1. Computer program to calculate D and DB^2.

Table A.1. Atom densities for the fuel elements

Characteristics	4.0% fuel type	3.3% fuel type
$A = \pi r^2 (cm^2)$	6.25754E-01	5.26814E-01
$\rho_e \left(\frac{gm}{cm^3}\right)$	10.21168	10.25029
$N_{U\text{-}Total} \left(\frac{atoms}{barn\text{-}cm}\right)$	2.27772E-02	2.28633E-02
$N_{U\text{-}234} \left(\frac{atoms}{barn\text{-}cm}\right)$	7.18300E-06	6.74455E-06
$N_{U\text{-}235} \left(\frac{atoms}{barn\text{-}cm}\right)$	9.27911E-04	7.65580E-04
$N_{U\text{-}236} \left(\frac{atoms}{barn\text{-}cm}\right)$	5.28400E-06	3.68959E-06
$N_{U\text{-}238} \left(\frac{atoms}{barn\text{-}cm}\right)$	2.18515E-02	2.20995E-02
$N_{O\text{-}16} \left(\frac{atoms}{barn\text{-}cm}\right)$	4.55544E-02	4.57262E-02

Table A.2. Atom densities for the SS-304 cladding of 4.0% fuel

SS-304 elements	Chemical composition w/0	$\rho_e \left(\frac{gm}{cm^3}\right)$	$N \left(\frac{atoms}{barn\text{-}cm}\right)$
Mn	1.29 $\pm$ 0.03	7.891	1.11600E-03
Cr	18.3 $\pm$ 0.4	7.891	1.67273E-02
Ni	10.03 $\pm$ 0.20	7.891	8.11960E-03
Fe	70.038 $\pm$ 0.711	7.891	5.96045E-02

Table A.3. Atom densities for the zircaloy cladding of 3.3% fuel

Zircaloy-4 element	Chemical composition w/0	$\rho_e\left(\frac{gm}{cm^3}\right)$	$N\left(\frac{atoms}{barn-cm}\right)$
Sn	1.41 ± 0.06	6.6456	4.75500E-04
Zr	98.17 ± 0.06	6.6456	4.30760E-02

Table A.4. Atom densities for the pyrex rod

Elements	Isotopic composition	(w/o) or (a/o)	$N\left(\frac{atoms}{barn-cm}\right)$
Si	Natural	100	1.75000E-02
B	B-10	19.775 ± 0.005	1.11430E-03
	B-11	80.225 ± 0.005	4.52070E-03
Al	Natural	100	5.80400E-04
Fe	Natural	100	8.40000E-06
Na	Natural	100	1.48630E-03
K	Natural	100	3.21200E-04
O_{Total}	Natural	100	4.52394E-02

Table A.5. Atom densities for the SS-304 pyrex cladding

SS-304 elements	Chemical composition w/0	$\rho_e\left(\frac{gm}{cm^3}\right)$	$N\left(\frac{atoms}{barn\text{-}cm}\right)$
Mn	0.87 ± 0.42	7.9 ± 0.1	7.53500E-04
Cr	18.4 ± 0.1	7.9 ± 0.1	1.68379E-02
Ni	9.5 ± 0.5	7.9 ± 0.1	7.69930E-03
Fe	70.84 ± 1.28	7.9 ± 0.1	6.03558E-02

Table A.6. Atom densities for the SS-304 baffle

SS-304 elements	Chemical composition w/0	$\rho_e\left(\frac{gm}{cm^3}\right)$	$N\left(\frac{atoms}{barn\text{-}cm}\right)$
Mn	1.371 ± 0.441	7.902 ± 0.004	1.18770E-03
Cr	16.37 ± 0.23	7.902 ± 0.004	1.49840E-02
Ni	8.72 ± 0.15	7.902 ± 0.004	7.06890E-03
Fe	72.745 ± 0.343	7.902 ± 0.004	6.19945E-02

Table A.7. Atom densities for H_2O

Water elements	$\rho_e\left(\frac{gm}{cm^3}\right)$	$N\left(\frac{atoms}{barn\text{-}cm}\right)$
H	1.0	6.68652E-02
O	1.0	3.34326E-02

Table A.8. Atom densities for the homogenized fuel cells

Composition		$N\left(\frac{\text{atoms}}{\text{barn-cm}}\right)$	
		4.0% fuel type	3.3% fuel type
Fuel	U-234	4.83120E-06	2.22330E-06
	U-235	3.65740E-04	2.54040E-04
	U-236	2.08270E-06	1.22780E-06
	U-238	8.61230E-03	7.33343E-03
	O	1.79550E-02	1.51735E-02
SS-304 cladding	Mn	7.88830E-05	-
	Cr	1.18235E-03	-
	Ni	5.73925E-04	-
	Fe	4.21310E-03	-
Zircaloy-4 cladding	Sn	-	4.78945E-05
	Zr	-	4.33881E-03
H_2O moderator	H	3.52260E-02	3.70110E-02
	O	1.76130E-02	1.85055E-02
	O_{Total}	3.55680E-02	3.36790E-02

Table A.9. Atom densities for the homogenized pyrex cell

Composition		$N\left(\frac{\text{atoms}}{\text{barn-cm}}\right)$
	Si	3.91030E-03
	B-10	2.48980E-04
	B-11	1.01010E-03
Pyrex	Al	1.29690E-04
	Fe	1.87690E-06
	Na	3.32105E-04
	K	7.17700E-05
	O	1.01085E-02
	Mn	2.71684E-05
SS-304	Cr	6.07112E-04
cladding	Ni	2.77610E-04
	Fe	2.17621E-03
H_2O	H	3.52260E-02
	O	1.76130E-02
	O_{Total}	2.77215E-02
	Fe_{Total}	2.17809E-03

Table A.10. Outer radii for the VENUS 1-D model

Zone	Radius (cm)
1	4.2508
2	7.1088
3	9.6288
4	21.3264
5	34.4184
6	35.4264
11	35.6784
12	35.9304
13	36.1824
14	36.4344
15	36.6864
16	36.9384
7	39.7964
8	48.2830
9	53.2500
10	64.7684

Table A.11. Calculated 10-group diffusion coefficients

	$D_{z,g}$ (cm)			
	Zones			
Group	1,15-18,20 (H_2O)	3,4-10 (3.3% fuel + pyrex)	11-13,21-26 (4.0% fuel)	2,14,19 (SS-304)
1	2.2534	2.3064	2.1771	1.7390
2	1.0544	1.1631	1.1600	1.7191
3	0.5936	0.6935	0.6968	0.9678
4	0.4181	0.5104	0.4947	0.4890
5	0.3870	0.4917	0.4731	0.3898
6	0.3879	0.4949	0.4605	0.3203
7	0.3851	0.4802	0.4494	0.3734
8	0.3686	0.4734	0.4454	0.3662
9	0.3334	0.4609	0.4357	0.3550
10	0.1324	0.2334	0.2267	0.3161

Table A.12. Calculated 56-group diffusion coefficients

Group	$D_{z,g}$ (cm)			
	Zones			
	1,15-18,20 (H_2O)	3,4-10 (3.3% fuel + pyrex)	11-13 (4.0% fuel)	2,14,19 (SS-304)
1	7.5008	4.4858	4.0506	2.3637
2	7.0258	4.3112	3.9175	2.3995
3	5.8587	3.8070	3.4732	2.3432
4	6.1662	3.9361	3.5881	2.3110
5	6.0367	3.8817	3.5470	2.2538
6	5.5458	3.6887	3.3687	2.2021
7	5.7308	3.7730	3.4469	2.1478
8	5.0142	3.4237	3.1467	2.0938
9	5.7221	3.7641	3.4465	2.0140
10	4.9375	3.4180	3.1242	1.8797
11	4.3262	3.1351	2.8785	1.7798
12	3.3303	2.5844	2.3880	1.7496
13	2.9988	2.3797	2.1994	1.7354
14	4.0100	3.0508	2.7985	1.7062
15	3.8991	2.9777	2.7405	1.6780
16	3.9077	2.9827	2.7269	1.5426
17	4.5454	3.3590	3.0874	1.6278
18	5.2304	3.7700	3.5494	1.8633
19	3.8827	3.0189	2.8057	1.7197
20	3.1645	2.5523	2.3747	1.6739
21	2.9749	2.4453	2.2727	1.6122
22	2.3235	1.9887	1.8725	1.7684
23	2.5436	2.1646	2.0436	1.7883
24	2.2690	1.9786	1.8564	1.5709
25	2.2182	1.9501	1.8546	1.6893
26	1.7762	1.6042	1.5303	1.5916
27	1.4610	1.3427	1.2995	2.0597
28	1.2341	1.1227	1.1041	2.2789
29	1.6912	1.5268	1.5279	2.0505
30	1.7228	1.5535	1.5294	1.3878
31	1.6747	1.5221	1.5499	2.0440
32	1.5925	1.4391	1.4796	1.8707
33	8.6454	0.8153	0.8068	1.3082
34	1.0331	0.9740	0.9852	1.8614
35	0.8962	0.8885	0.8897	1.1490

Table A.12. Continued

Group	$D_{z,g}$ (cm)			
	Zones			
	1,15-18,20 (H_2O)	3,4-10 (3.3% fuel + pyrex)	11-13 (4.0% fuel)	2,14,19 (SS-304)
36	0.9715	0.9423	0.9261	0.8945
37	0.8962	0.8885	0.8897	1.1490
38	0.8300	0.8376	0.8125	0.7025
39	0.8066	0.8200	0.8012	0.7479
40	0.7740	0.7950	0.7991	1.0437
41	0.7211	0.7519	0.7407	0.7925
42	0.6836	0.7238	0.6993	0.5934
43	0.6641	0.7074	0.6267	0.2643
44	0.6513	0.6970	0.7121	1.6934
45	0.6455	0.6923	0.7030	1.4453
46	0.6329	0.6819	0.6680	0.7235
47	0.6190	0.6700	0.6404	0.5 50
48	0.6074	0.6599	0.6102	0.375
49	0.5990	0.6450	0.5863	0.306
50	0.5932	0.6166	0.5792	0.3280
51	0.5891	0.6017	0.5917	0.3943
52	0.5864	0.6397	0.5742	0.3496
53	0.5818	0.6458	0.5867	0.3582
54	0.5800	0.6476	0.5842	0.3739
55	0.5781	0.6605	0.5964	0.3654
56	0.5602	0.2431	0.2313	0.3013

Table A.13. Calculated 56-group axial leakage approximation values

	$[DB^2]_{z,g}$ (cm^{-1})			
	Zones			
Group	1,15-18,20 (H_2O)	3,4-10 (3.3% fuel + pyrex)	11-13 (4.0% fuel)	2,14,19 (SS-304)
1	1.8002E-02	1.0766E-02	9.7214E-03	5.6730E-03
2	1.6862E-02	1.0347E-02	9.4019E-03	5.7589E-03
3	1.4061E-02	9.1368E-03	8.3558E-03	5.6237E-03
4	1.4799E-02	9.4466E-03	8.6115E-03	5.5465E-03
5	1.4488E-02	9.3314E-03	8.5129E-03	5.4092E-03
6	1.3310E-02	8.8528E-03	8.0849E-03	5.2850E-03
7	1.3754E-02	9.0553E-03	8.2725E-03	5.1548E-03
8	1.2034E-02	8.2169E-03	7.5522E-03	5.0252E-03
9	1.3733E-02	9.0339E-03	8.2715E-03	4.8336E-03
10	1.1850E-02	8.2032E-03	7.4981E-03	4.5113E-03
11	1.0383E-02	7.5242E-03	6.9085E-03	4.3196E-03
12	7.9927E-03	6.2025E-03	5.7312E-03	4.1991E-03
13	7.1972E-03	5.7113E-03	5.2786E-03	4.1649E-03
14	9.6241E-03	7.3220E-03	6.7165E-03	4.0950E-03
15	9.3578E-03	7.1465E-03	6.5772E-03	4.0273E-03
16	9.3784E-03	7.1586E-03	6.5446E-03	3.7022E-03
17	1.0909E-02	8.0616E-03	7.4097E-03	3.9067E-03
18	1.2553E-02	9.0481E-03	8.5186E-03	4.4719E-03
19	9.3185E-03	7.2454E-03	6.7336E-03	4.1273E-03
20	7.5947E-03	6.1256E-03	5.6993E-03	4.0173E-03
21	7.1398E-03	5.8687E-03	5.4545E-03	3.8692E-03
22	5.5765E-03	4.7729E-03	4.4940E-03	4.2442E-03
23	6.1046E-03	5.1950E-03	4.9046E-03	4.2920E-03
24	5.4456E-03	4.7487E-03	4.4553E-03	3.7701E-03
25	5.3238E-03	4.6802E-03	4.4512E-03	4.0544E-03
26	4.2629E-03	3.8502E-03	3.6728E-03	3.8199E-03
27	3.5065E-03	3.2224E-03	3.1188E-03	4.9434E-03
28	2.9618E-03	2.6945E-03	2.6498E-03	5.4693E-03
29	4.0590E-03	3.6643E-03	3.6669E-03	4.9211E-03
30	4.1347E-03	3.7283E-03	3.6706E-03	3.3307E-03
31	4.0193E-03	3.6531E-03	3.7198E-03	3.9056E-03
32	3.8221E-03	3.4538E-03	3.5510E-03	4.4897E-03
33	2.0749E-03	1.9567E-03	1.9364E-03	3.1398E-03
34	2.4794E-03	2.3377E-03	2.3646E-03	4.4674E-03
35	2.4601E-03	2.3486E-03	2.3671E-03	3.3954E-03

Table A.13. Continued

Group	$[DB^2]_{z,g}$ (cm^{-1})			
	Zones			
	1,15-18,20 (H_2O)	3,4-10 (3.3% fuel + pyrex)	11-13 (4.0% fuel)	2,14,19 (SS-304)
36	2.3317E-03	2.2615E-03	2.2226E-03	2.1469E-03
37	2.1510E-03	2.1324E-03	2.1354E-03	2.7575E-03
38	1.9920E-03	2.0103E-03	1.9500E-03	1.6860E-03
39	1.9358E-03	1.9681E-03	1.9229E-03	1.7949E-03
40	1.8576E-03	1.9081E-03	1.9179E-03	2.5050E-03
41	1.7307E-03	1.8045E-03	1.7776E-03	1.9019E-03
42	1.6407E-03	1.7371E-03	1.6784E-03	1.4242E-03
43	1.5938E-03	1.6978E-03	1.5040E-03	6.3442E-04
44	1.5632E-03	1.6727E-03	1.7091E-03	4.0642E-03
45	1.5493E-03	1.6615E-03	1.6871E-03	3.4688E-03
46	1.5189E-03	1.6365E-03	1.6031E-03	1.7365E-03
47	1.4855E-03	1.6079E-03	1.5370E-03	1.2621E-03
48	1.4577E-03	1.5837E-03	1.4645E-03	0.0158E-04
49	1.4375E-03	1.5481E-03	1.4071E-03	7.3614E-04
50	1.4236E-03	1.4798E-03	1.3901E-03	7.8722E-04
51	1.4138E-03	1.4442E-03	1.4201E-03	9.4641E-04
52	1.4074E-03	1.5352E-03	1.3780E-03	8.3906E-04
53	1.3963E-03	1.5500E-03	1.4081E-03	8.5960E-04
54	1.3921E-03	1.5543E-03	1.4021E-03	8.9737E-04
55	1.3875E-03	1.5852E-03	1.4314E-03	8.7693E-04
56	1.3446E-03	5.8339E-04	5.5521E-04	7.2317E-04

NUREG/CR-3888
ORNL/TM-9238
Dist. Category R5

INTERNAL DISTRIBUTION

1. C. A. Baldwin
2. J. Debrue
3. D. M. Eissenberg
4. A. Fabry
5-11. F. B. K. Kam
12. L. Leenders
13. R. E. Maerker
14. A. P. Malinauskas
15. L. F. Miller
16. G. Minsart
17-19. P. O. Morakinyo
20. J. A. Setaro
21. F. W. Stallmann
22. J. H. Swanks
23. M. L. Williams
24. Document Reference Section
25-27. Central Research Library
28. Laboratory Records Department
29. Laboratory Records - ORNL R.C.
30. ORNL Patent Office

EXTERNAL DISTRIBUTION

30. Assistant Manager for Energy Research and Development, U.S. Department of Energy, Oak Ridge Operations Office, Oak Ridge TN 37830
31-32. Technical Information Center, U.S. Department of Energy, Oak Ridge TN 37830
33-382. Given distribution under category R5 (10 copies - NTIS)

NRC FORM 335 (11-81)

U.S. NUCLEAR REGULATORY COMMISSION

BIBLIOGRAPHIC DATA SHEET

1. REPORT NUMBER (Assigned by DDC)
NUREG/CR-3888
ORNL/TM-9238

4. TITLE AND SUBTITLE (Add Volume No., if appropriate)
ANALYSIS OF THE VENUS PWR ENGINEERING MOCKUP EXPERIMENT - PHASE I: SOURCE DISTRIBUTION

2. (Leave blank)

3. RECIPIENT'S ACCESSION NO.

7. AUTHOR(S)
P. O. Morakinyo, M. L. Williams, and F. B. K. Kam

5. DATE REPORT COMPLETED
MONTH June YEAR 1984

9. PERFORMING ORGANIZATION NAME AND MAILING ADDRESS (Include Zip Code)
Oak Ridge National Laboratory
P. O. Box X
Oak Ridge, Tennessee 37831

DATE REPORT ISSUED
MONTH YEAR

6. (Leave blank)

8. (Leave blank)

12. SPONSORING ORGANIZATION NAME AND MAILING ADDRESS (Include Zip Code)
Division of Engineering Technology
Office of Nuclear Regulatory Research
U.S. Nuclear Regulatory Commission
Washington, D.C. 20555

10. PROJECT/TASK/WORK UNIT NO.

11. FIN NO
B0415

13. TYPE OF REPORT
Topical

PERIOD COVERED (Inclusive dates)
June 1984

15. SUPPLEMENTARY NOTES

14. (Leave blank)

16. ABSTRACT (200 words or less)

The neutron fission source distribution in the core of the VENUS PWR Mockup Experiment is computed and compared to experimental measurements. Of particular concern is the accuracy of the source calculation near the core-baffle interface, which is the important region for contributing to RPV fluence.

Results indicate that the calculated neutron source distribution within the VENUS core agrees with the experimentally measured values with an average error of less than 3%. At the important core-baffle interface, the agreement is within 3% error, except at the baffle corner, where the error is about 6%. Better accuracy in the calculations can be obtained by applying a detailed space dependent cross-section weighting procedure to the core-baffle interface region. Using this cross-section weighting, the maximum error introduced into the predicted RPV fluence due to source errors should be on the order of 5%. However, in power reactor analysis, additional complexities (such as the time-dependent core composition and the use of few group diffusion theory) could affect this uncertainty value.

17. KEY WORDS AND DOCUMENT ANALYSIS

17a. DESCRIPTORS

17b. IDENTIFIERS/OPEN-ENDED TERMS

18. AVAILABILITY STATEMENT
Unlimited

19. SECURITY CLASS (This report)
Unclassified

21. NO. OF PAGES

20. SECURITY CLASS (This page)
Unclassified

22. PRICE
$

NRC FORM 335 (11-81)